CHEMISTRY OF MATERIALS
Article

Chem. Mater. **2010,** *22,* 6347–6360 6347
DOI:10.1021/cm102263s

PEGylated Imidazolium Ionic Liquid Electrolytes: Thermophysical and Electrochemical Properties

Lalitha V. N. R. Ganapatibhotla,[†] Jianping Zheng,[‡] Dipankar Roy,[‡] and Sitaraman Krishnan*,[†]

[†]*Department of Chemical and Biomolecular Engineering and* [‡]*Department of Physics, Clarkson University, Potsdam, New York 13699, United States*

Received August 9, 2010. Revised Manuscript Received October 17, 2010

We report the synthesis and characterization of a series of imidazolium iodide ionic liquids (ILs) containing monomethoxy-terminated poly(ethylene glycol) (mPEG), and *n*-alkyl groups. These PEGylated ILs contain 7, 12, or 16 ethylene glycol units in the side chains, and are designed as potential electrolytes for energy conversion and storage devices such as dye-sensitized solar cells, supercapacitors, and Li ion batteries. The thermophysical (density, viscosity, and the temperatures of glass-transition, crystallization and melting) and electrochemical (nonfaradaic window, and capacitor leakage resistance) properties of the ILs, that are critical to these targeted applications, are studied using an array of techniques. 1-Alkyl-3-methylimidazolium iodide ILs are synthesized and characterized in parallel with the PEGylated ILs, to compare how the electrolyte properties of the two systems are affected by their detailed molecular structures, and especially by the ether oxygen atoms. The mPEG side chains show strong intramolecular interactions with the imidazolium ring, weakening Coulombic interactions between the imidazolium cation and the iodide anion. The PEGylated ILs, therefore, exhibit conductivities of the order of 0.1 mS cm^{-1} (25 °C) despite their relatively high viscosities, and support a temperature-independent electrochemical window of about 2 V, demonstrating their suitability for extended temperature applications.

1. Introduction

Electrolytes based on organic solvents are commonly used in electrochemical energy storage and conversion devices, such as dye-sensitized solar cells (DSSCs), supercapacitors, and lithium ion batteries. However, because of their volatility and flammability, these liquids tend to limit the long-term stability and high temperature operation of the devices.[1] Thermal expansion often results in leakage of liquid electrolytes when the devices are operated at elevated temperatures. To address these problems, a variety of solid and quasi-solid materials have been proposed as alternative electrolytes for different electrochemical power cells.[2−9] Many of these devices, however, use nanoporous electrode materials, and obtaining an adequate electrode−electrolyte contact is difficult while using single-phase solid electrolytes.[10] As a result, quasi-solid and gel electrolytes have attracted considerable attention, and those based on ionic liquids (ILs) have become particularly popular because of the intensified ion densities, good ionic conductivities, and wide electrochemical windows of these room-temperature molten salts.[1−12] Our present work focuses on the synthesis and the physicochemical characterization of certain IL electrolytes that are capable of nanoscale segregation and gelation, and which could be useful in improving the operational temperature range, as well as the long-term stability of DSSCs.

We have selected imidazolium (Im) based ionic liquids for our study because this general class of electrolytes appears to be promising for various electrochemical applications. The relatively easy quaternization of the imidazole ring nitrogen, and the straightforward metathesis reactions for anion exchange, provide a wide range of chemical structures for these ILs, of which the 1,3-dialkylimidazolium (C_mC_nIm) cation has been widely studied.[2−5,13−17] We report here the synthesis

*To whom correspondence should be addressed. E-mail: skrishna@clarkson.edu.

(1) Kuang, D.; Klein, C.; Zhang, Z.; Ito, S.; Moser, J. E.; Zakeeruddin, S. M.; Grätzel, M. *Small* **2007**, *3*, 2094.
(2) Echelmeyer, T.; Meyer, H. W.; Wüllen., L. V. *Chem. Mater.* **2009**, *21*, 2280.
(3) Letaief, S.; Diaco, T.; Pell, W.; Gorelsky, S. I.; Detellier, C. *Chem. Mater.* **2008**, *20*, 7136.
(4) Shimano, S.; Zhou, H.; Honma, I. *Chem. Mater.* **2007**, *19*, 5216.
(5) Néouze, M.-A.; Bideau, J. L.; Gaveau, P.; Bellayer, S.; Vioux, A. *Chem. Mater.* **2006**, *18*, 3931.
(6) Joseph, J.; Son, K. M.; Vittal, R.; Lee, W.; Kim, K.-J. *Semicond. Sci. Technol.* **2006**, *21*, 697.
(7) Wang, Q.; Zakeeruddin, S. M.; Exnar, I.; Grätzel, M. *J. Electrochem. Soc.* **2004**, *151*, A1598.
(8) Sivaraman, P.; Hande, V. R.; Mishra, V. S.; Srinivasa Rao, Ch.; Samui, A. B. *J. Power Sources* **2003**, *124*, 351.
(9) Lin, B.; Cheng, S.; Qiu, L.; Yan, F.; Shang, S.; Lu, J. *Chem. Mater.* **2010**, *22*, 1807.
(10) Dai, Q.; MacFarlane, D. R.; Forsyth, M. *Solid State Ionics* **2006**, *177*, 395.
(11) Castner, E. W.; Wishart, J. F. *J. Chem. Phys.* **2010**, *132*, 120901.
(12) Mayrand-Provencher, L.; Rochefort, D. *J. Phys. Chem. C* **2009**, *113*, 1632.
(13) Sekhon, S. S.; Park, J.-S.; Baek, J.-S.; Yim, S.-D.; Yang, T.-H.; Kim, C.-S. *Chem. Mater.* **2010**, *22*, 803.
(14) Döbbelin, M.; Marcilla, R.; Salsamendi, M.; Pozo-Gonzalo, C.; Carrasco, P. M.; Pomposo, J. A.; Mecerreyes, D. *Chem. Mater.* **2007**, *19*, 2147.
(15) McEwen, A. E.; Ngo, H. L.; LeCompte, K.; Goldman, J. L. *J. Electrochem. Soc.* **1999**, *146*, 1687.
(16) Egashira, M.; Todo, H.; Yoshimoto, M.; Morita, M.; Yamaki, J. *J. Power Sources* **2007**, *174*, 560.

Published on Web 11/12/2010

and characterization of new poly(ethylene glycol) (PEG) functionalized Im iodides.

There is significant fundamental and practical interest in designing ILs with polar and nonpolar side chains.[18−22] Molecular dynamics simulations of ether-derivatized Im-based ionic liquids have shown that, the ether oxygen atoms can associate with the hydrogen atoms of the Im ring to weaken ionic interactions between the Im cation and anions such as bis(trifluoromethylsulfonyl)imide (Tf_2N) and tetrafluoroborate (BF_4), resulting in increased fluidity of the ILs.[19−21] The weakened cation−anion interactions in ether-derivatized ionic liquids makes them attractive for various applications that require high ionic conductivity. Recently, Luo et al. have reported the formation of 1:1 self-assembled complexes in physical blends of C_nMeImBF$_4$, and PEG, with 18 ethylene oxide units in the polymer chain.[23] Using experimental results from electrospray ionization mass spectrometry, they proposed that PEG wrapped around the imidazolium ring, because of interactions of ether oxygen atoms with the ring, but how the viscosity or ionic conductivity was influenced by the PEG−Im complex formation has not been studied.

The influence of covalently attached, relatively long polyether tails on the physicochemical and transport properties of Im ILs is therefore an intriguing topic that needs further investigation. The new ILs synthesized in this work consist of monomethoxy-terminated poly(ethylene glycol) (mPEG) side chains with a relatively large number of ether oxygen atoms. Considering their target application as redox couples in DSSCs, iodide was selected as the anion in the Im ILs. Of the different mediators available for electron transfer between the cathode and the anode, the iodide/triiodide redox couple is the material of choice for DSSCs because of properties such as rapid dye regeneration, fast charge transport, and slow recombination kinetics between the electrons in TiO_2 and the triiodide.[24] Furthermore, it has been shown that the power conversion efficiency of a DSSC that used an IL as solvent for the I^-/I_3^- redox couple was higher than a DSSC that used a nonionic "molecular" liquid as the solvent, because of higher diffusion coefficients of the redox ions, attributed to the kinetic electrolyte effect of the solvent ions.[25] Because of these interesting features of IL electrolytes in general, and the I^-/I_3^- mediator in particular, our investigation is aimed at long-chain mPEG-derivatized imidazolium iodide ILs. For practical applications, an optimized balance between the viscosity and the ionic conductivity of these ILs is necessary, which can be achieved by utilizing the polar nature and self-assembly of the mPEG tails.

Polymer gel electrolytes based on poly(ethylene oxide) and PEG have been reported previously,[26−31] but imidazolium iodide salts with different lengths of PEG tails have not been studied. Likewise, quantitative physicochemical characterization of C_nMeImI have been discussed in only few reports,[32,33] while the corresponding case of PEGylated imidazolium iodides has remained even less explored. In the present work, we synthesized these PEGylated ILs, and performed a series of multitechnique measurements to establish certain physicochemical behaviors of these electrolytes that are essential for DSSC operation. For comparison with these ILs, a number of C_nMeImI ionic liquids are also synthesized and characterized. This comparison is primarily aimed at understanding the influence of the PEG oxygen atoms on the IL properties.

The material compositions of the experimental ILs are examined here using NMR spectroscopy, and the general electrolyte properties are characterized in terms of their temperature-dependent viscosities, and conductivities. The mechanisms that dictate the temperature dependent viscosities and conductivities of the ILs are examined in a framework of commonly used phenomenological models. The thermal stabilities of the ILs are determined through thermogravimetry, whereas their glass-transition, crystallization, and melting temperatures are obtained using differential scanning calorimetry (DSC). Selected electrolytes, taken as representative samples from the series of the synthesized ILs, are subjected to electrochemical characterization. Cyclic voltammetry (CV) is employed to determine the electrochemical windows of the IL electrolytes at a glassy carbon (GC) working electrode, as well as to estimate the double layer capacitances at the GC−IL interfaces between 25 and 75 °C (covering the expected temperature range of DSSC operation). Electrochemical impedance spectroscopy (EIS), combined with complex nonlinear least-squares (CNLS) analysis of the EIS data provides electrode equivalent circuit (EEC) models of these GC−IL systems, which in turn, provides the polarization (capacitor leakage) resistance at different temperatures between 25 and 75 °C. These CV and EIS results are used to evaluate the overall electrochemical stabilities, as well as the general electrode-interface-forming characteristics of the experimental ILs.

(17) Bonhôte, P.; Dias, A.-P.; Papageorgiou, N.; Kalyanasundaram, K.; Grätzel, M. *Inorg. Chem.* **1996**, *35*, 1168.
(18) Niedermeyer, H.; Ab Rani, M. A.; Lickiss, P. D.; Hallett, J. P.; Welton, T.; White, A. J. P.; Hunt, P. A. *Phys. Chem. Chem. Phys.* **2010**, *12*, 2018.
(19) Smith, G. D.; Borodin, O.; Li, L.; Kim, H.; Liu, Q.; Bara, J. E.; Gin, D. L.; Nobel, R. *Phys. Chem. Chem. Phys.* **2008**, *10*, 6301.
(20) Zhou, Z.-B.; Matsumoto, H.; Tatsumi, K. *Chem.—Eur. J.* **2006**, *12*, 2196.
(21) Branco, L. C.; Rosa, J. N.; Ramos, J. J. M.; Afonso, C. A. M. *Chem.—Eur. J.* **2002**, *8*, 3671.
(22) Jovanovski, V.; Stathatos, E.; Orel, B.; Lianos, P. *Thin Solid Films* **2006**, *511−512*, 634.
(23) Luo, S.; Zhang, S.; Wang, Y.; Xia, A.; Zhang, G.; Du, X.; Xu, D. *J. Org. Chem.* **2010**, *75*, 1888.
(24) Boschloo, G.; Hagfeldt, A. *Acc. Chem. Res.* **2009**, *42*, 1819.
(25) Kawano, R.; Watanabe, M. *Chem. Commun.* **2005**, 2107.
(26) Li, F.; Cheng, F.; Shi, J.; Cai, F.; Liang, M.; Chen, J. *J. Power Sources* **2007**, *165*, 911.
(27) Shim, H. J.; Kim, D. W.; Lee, C.; Kang, Y.; Suh, D. H. *Macromol. Res.* **2008**, *16*, 424.
(28) Kang, M.-S.; Kim, J. H.; Kim, Y. J.; Won, J.; Park, N.-G.; Kang, Y. S. *Chem. Commun.* **2005**, 889.
(29) Kang, M.-S.; Kim, J. H.; Won, J.; Kang, Y. S. *J. Phys. Chem. C* **2007**, *111*, 5222.
(30) Klingshirn, M. A.; Spear, S. K.; Subramanian, R.; Holbrey, J. D.; Huddleston, J. G.; Rogers, R. D. *Chem. Mater.* **2004**, *16*, 3091.
(31) Freitas, F. S.; de Freitas, J. N.; Ito, B. I.; De Paoli, M.-A.; Nogueira, A. F. *ACS Appl. Mater. Interfaces* **2009**, *1*, 2870.
(32) Kubo, W.; Kitamura, T.; Hanabusa, K.; Wada, Y.; Yanagida, S. *Chem. Commun.* **2002**, 374.
(33) Fei, Z.; Kuang, D.; Zhao, D.; Klein, C.; Ang, W. H.; Zakeeruddin, S. M.; Grätzel, M.; Dyson, P. J. *Inorg. Chem.* **2006**, *45*, 10407.

2. Experimental Section

2.1. Materials. Methoxy-terminated polyethylene glycols ($CH_3O(CH_2CH_2O)_nH$, mPEG*n*, $\langle n \rangle$ = 7, 12, and 16, CAS no. 9004−74−4), *p*-toluenesulfonyl chloride (TsCl, CAS no. 98−59−9, 99%), anhydrous sodium iodide (CAS no.7681−82−5, 99.999%), 1-methylimidazole (CAS no. 616−47−7, 99%), 1-butylimidazole (CAS no. 4316−42−1, 98%), 1-iodoethane (CAS no. 75−03−6, 99%) 1-iodopropane (CAS no.107−08−4, 99%), 1-iodobutane (CAS no. 542−69−8, 99%), 1-iodohexane (CAS no. 638−45−9, 98%), and lithium iodide hydrate (CAS no. 85017−80−7, 98%), obtained from Sigma-Aldrich, were used without further purification. 1-Ethyl-3-methylimidazolium ethylsulfate ($EtMeImEtSO_4$, ECOENG212, Solvent Innovation) was vacuum-dried at 80 °C before use. Anhydrous pyridine, methylene chloride, acetone, *N,N*-dimethylformamide (DMF), sodium bicarbonate, hydrochloric acid, sodium thiosulfate, and anhydrous sodium sulfate (all from Fisher), and diethyl ether (Et_2O, Alfa Aesar) were also used as received.

2.2. Synthesis of 1-(Methoxy PEG)-3-methylimidazolium Iodides (mPEG*n*MeImI). The synthesis of the mPEG12MeImI is described here. The other three PEGylated ionic liquids were synthesized in a similar manner.

Tosylation of methoxy-terminated poly(ethylene glycol). mPEG12 ($CH_3O(CH_2CH_2O)_{12}H$, 17.56 g, 31 mmol) was mixed with anhyd. pyridine (4.75 g, 60 mmol) in a round-bottom flask, and a solution of TsCl (12.75 g, 67 mmol) in anhyd. CH_2Cl_2 (45 mL) was added dropwise to the flask while cooling the flask in an ice-bath (∼ 0 °C). A white precipitate formed immediately after the addition of TsCl. After 1 h, the reaction mixture was warmed back to room temperature. After 24 h of mixing at room temperature, CH_2Cl_2 (50 mL) was added to the reaction flask and the resulting mixture was stirred for 30 min, followed by sequential extractions with satd. $NaHCO_3$ soln. (3 × 30 mL), 1 M aq. HCl soln. (3 × 30 mL), and distilled water (3 × 30 mL). The organic layer was dried over sodium sulfate, filtered, and concentrated by evaporation of CH_2Cl_2 under vacuum. The resulting colorless liquid was dried in vacuo for about 12 h. This liquid (17.71 g) contained about 89.3 mol % of mPEG12 tosylate and 10.7 mol % of the starting mPEG12. The yield of mPEG12 tosylate, based on the initial amount of mPEG12 was, therefore, ∼ 72%. The mixture was used in the next step, without further purification. ^{1}H NMR (400 MHz, $CDCl_3$, δ): 7.80 and 7.35 (A_2B_2 dd, J = 8.2 Hz, 4H, aryl ring), 4.16 (t, J = 4.8 Hz, 2H, CH_2OTs), 3.5−3.8 (br m, CH_2CH_2O), 3.38 (s, 3.36H, OCH_3), 2.45 (s, 3H, Ar−CH_3).

Iodination of mPEG tosylate. NaI (8.79 g, 58.6 mmol) was added in the dark, with vigorous stirring, to mPEG12 tosylate (10.51 g, 13.6 mmol mPEG12 tosylate) dissolved in dry acetone (50 mL), and the resulting yellow mixture was stirred for 24 h under reflux at about 60 °C. A yellow solid eventually settled down in the reaction flask. After evaporating acetone using a rotary evaporator, CH_2Cl_2 (60 mL) and distd. water (40 mL) were added to the solid left behind in the flask. The mixture was stirred for 30 min at room temperature. The organic and aqueous phases were separated and the organic phase was extracted with 5% aq. $Na_2S_2O_3$ soln. (3 × 50 mL). The organic phase was further washed with satd. $NaHCO_3$ soln. (3 × 50 mL) and with distd. water (3 × 50 mL) and dried over sodium sulfate. The sodium sulfate was removed by filtration and CH_2Cl_2 was evaporated under vacuum. The product was further dried in a vacuum oven at 50 °C to obtain 8.95 g of a viscous liquid which contained 95.7 mol % of mPEG12 iodide and 4.3 mol % of mPEG12. This mixture was used in the next reaction without further purification. ^{1}H NMR (400 MHz, $CDCl_3$, δ): 3.26 (t, J = 6.9 Hz, 1.9H, CH_2I), 3.37 (s, 3H, OCH_3), 3.55 (t, J = 4.6 Hz, CH_2OCH_3), 3.52−3.71 (br m, CH_2CH_2O), 3.76 (t, J = 6.9 Hz, 1.9H, OCH_2CH_2I).

Quaternization of 1-Alkylimidazole Using mPEG Iodide. 1-Methylimidazole (1.76 g, 21 mmol) was added to a nitrogen-purged round-bottom flask containing mPEG12I (7.03 g, 10.7 mmol) in DMF (4 mL) and the mixture was stirred at 80 °C under nitrogen for 48 h. After cooling to room temperature, the reaction mixture was added slowly to cold (∼ 0 °C) Et_2O with vigorous stirring, which resulted in phase separation of the product. The top Et_2O layer was decanted off, and the product was repeatedly washed with fresh Et_2O, after which it was dried in vacuo for about 12 h to obtain 5.75 g of the pure IL. ^{1}H NMR (400 MHz, $CDCl_3$, δ): 3.38 (br s, 3H, OCH_3), 3.55 (t, J = 4.6 Hz, CH_2OCH_3), 3.52−3.70 (br m, 44.9H, CH_2CH_2O), 3.92 (t, J = 4.6 Hz, 2H, $N^+CH_2CH_2O$), 4.05 (s, 3H, NCH_3), 4.59 (t, J = 4.6 Hz, 2H, N^+CH_2), 7.46 (t, J = 1.6 Hz, 1H, NCH), 7.77 (s, 1H, N^+CH), 9.78 (s, 1H, N^+CHN).

2.3. Synthesis of 1-Alkyl-3-methylimidazolium Iodides. C_nMeImI ILs were synthesized using 1-methylimidazole and 1-iodoalkanes, using procedures similar to those reported previously.[17] The alkyl iodide (1-iodohexane, 1-iodobutane, or 1-iodopropane) was added dropwise, over a period of 1 h, to 1-methylimidazole taken in a round-bottom flask that was purged with dry nitrogen. The contents of the flask turned green (or yellow) immediately upon adding the alkyl iodide. The mixture was heated at 80 °C for 48 h period, and later cooled to room temperature and added dropwise to cold Et_2O with vigorous stirring. The top Et_2O layer was decanted off, and the extraction with Et_2O was repeated several times. The bottom layer was dried in vacuo at 50 °C, for about 12 h, to obtain a viscous liquid of high purity (determined using ^{1}H NMR). EtMeImI was recovered as a yellowish white powder after precipitation and washing with cold Et_2O. The powder was dissolved in chloroform, precipitated again in cold Et_2O, filtered, and dried in vacuo at 50 °C for about 12 h.

EtMeImI: ^{1}H NMR (400 MHz, $CDCl_3$, δ): 1.64 (t, J = 7.4 Hz, 3H, $N^+CH_2CH_3$), 4.13 (s, 3H, NCH_3), 4.42 (q, J = 7.5 Hz, 2H, N^+CH_2), 7.50 (apparent br d, J = 1.6 Hz, 2H, $NCHCHN^+$), 10.07 (s, 1H, N^+CHN).

PrMeImI: ^{1}H NMR (400 MHz, $CDCl_3$, δ): 1.02 (t, J = 7.4 Hz, 3H, N^+ $(CH_2)_2CH_3$), 2.0 (sx, J = 7.4 Hz, 2H, $N^+CH_2CH_2CH_3$), 4.14 (s, 3H, NCH_3), 4.32 (t, J = 7.2 Hz, 2H, $N^+CH_2CH_2$), 7.49 (s, J = 1.6 Hz, 1H, NCH), 7.55 (s, J = 1.6 Hz, 1H, N^+CH), 10.06 (s, 1H, N^+CHN).

BuMeImI: ^{1}H NMR (400 MHz, $CDCl_3$, δ): 0.98 (t, J = 7.4 Hz, 3H, N^+ $(CH_2)_3CH_3$), 1.41 (sx, J = 7.4 Hz, 2H, $N^+(CH_2)_2CH_2CH_3$), 1.93 (qn, J = 7.4 Hz, 2H, $N^+CH_2CH_2CH_2CH_2$), 4.14 (s, 3H, NCH_3), 4.34 (t, J = 7.4 Hz, 2H, $N^+CH_2CH_2CH_2$), 7.40 (t, J = 1.7 Hz, 1H, NCH), 7.48 (t, J = 1.7 Hz, 1H, N^+CH), 10.14 (s, 1H, N^+CHN).

HexMeImI: ^{1}H NMR (400 MHz, $CDCl_3$, δ): 0.88 (t, J = 7.0 Hz, 3H, $N^+(CH_2)_5CH_3$), 1.33 (br m, 6H, $N^+CH_2CH_2(CH_2)_3CH_3$), 1.93 (qn, J = 7.5 Hz, 2H, $N^+CH_2CH_2CH_2CH_2$), 4.13 (s, 3H, NCH_3), 4.32 (t, J = 7.5 Hz, 2H, N^+CH_2), 7.36 (t, J = 1.7 Hz, 1H, NCH), 7.45 (t, J = 1.7 Hz, 1H, N^+CH), 10.17 (s, 1H, N^+CHN).

2.4. Characterization. The chemical structures of the electrolytes were characterized using ^{1}H NMR Spectroscopy. A Bruker Avance 400 MHz NMR spectrometer was used to record ^{1}H NMR spectra of the salts in anhyd. deuterated chloroform (99.8 atom % D, 0.03% v/v tetramethylsilane, TMS), and chemical shifts are expressed in parts per million relative to TMS. Thermal degradation was studied using a Perkin-Elmer Pyris 1 Thermogravimetric Analyzer. The sample (∼ 30 mg) was heated in a Pt pan, under nitrogen purge, over a temperature range of 40−600 °C, at a rate of 15 °C/min. Thermal phase behavior was studied using a TA Instruments DSC Q100. The samples (10−15 mg) were weighed in aluminum pans and sealed with lids that contained pin holes. Thermal scans were performed in a nitrogen atmosphere over a temperature range of −80 to 100 °C (up to 120 °C for C_mC_nImI).

The sample temperature was ramped to 100 °C, held at this value for 10 min, decreased from 100 to −80 °C at a rate of 20 °C/min, held at −80 °C for 2 min, and finally heated from −80 to 80 °C at a rate of 2 °C/min. Data were collected during the first cooling and second heating steps.

The densities of ILs were determined at 25 ± 0.5 °C using an Ohaus microbalance (model DV215CD), with a resolution of 0.01 mg and 250 μL airtight syringe (Hamilton Co. Inc.). At least 5 measurements were made for each ionic liquid. The viscosities of the ionic liquids were determined over a temperature range of 20−95 °C (40−95 °C for EtMeImI) in steps of 5 °C using a Brookfield LVDV-II+Pro model cone and plate viscometer installed with a model CP 52 cone spindle (4.6 cP to 9.2×10^4 cP range). The ILs were dried for 24 h in a vacuum oven, at 50 °C prior to the viscosity experiment. The viscometer was sealed with a Teflon tape to prevent the absorption of moisture by the system during the experiment, and measurements (at each temperature) were first carried out at different rotational speeds of the spindle, to confirm Newtonian flow behavior.

Ionic conductivities of the electrolytes were determined, at temperatures between 10 and 100 °C, using EIS in a cylindrical chamber cell designed and assembled in our laboratory. This cell, consisting of two identical flat electrodes of stainless steel in Teflon housing, was thermally controlled inside a TESTEQUITY 105A environmental chamber. The test cell was sealed with a Teflon tape after loading the sample. Activated silica gel was placed in the environmental chamber during these experiments to minimize moisture absorption by the sample during conductivity measurements. The IL conductivity, at any given temperature, did not vary with the time spent in the environmental chamber, which indicated satisfactory humidity control in these experiments. EIS data were recorded as Nyquist plots with 15 mV amplitude A.C. perturbation voltages at selected frequencies between 0.3 and 30 kHz, by using a Solartron 1287A potentiostat/galvanostat, coupled with a model 1252A frequency response analyzer. Experimental Nyquist spectra were validated through Kramers−Kronig (KK) transform procedures, and CNLS-analyzed to obtain the appropriate electrode equivalent circuit (EECs) model for evaluating the bulk resistance (R_s) and hence the conductivity of the test electrolytes. ZSimpWin was used for both the KK and the CNLS fitting calculations. The uncertainties in all the calculated impedance elements were < 5%. The geometric constant, L/A, of the conductivity cell was determined using a standard KCl solution, resulting in a value of 0.22 cm^{-1} (L and A denote the spacing and the surface area of the electrodes, respectively). The resistivity, ρ, and hence, the conductivity, λ, was determined using $\rho = 1/\lambda = R_s(L/A)^{-1}$.

Three electrode cells were used for the measurements of electrochemical stability windows and impedance spectra. Only voltage ranges (rather than absolute reaction potentials) were necessary in the determination of electrolytic stability, and all the EIS data were recorded at OCPs. Ag or Pt wire quasi-reference electrodes are frequently used for such measurements,[34−36] and this approach was adapted in the present work. Electrochemical windows were determined with D.C. CV, at a scan rate of 50 mVs^{-1}, using a home-built three-electrode glass cell containing 0.5 mL electrolyte, a GC working electrode, a Pt wire (2 mm diameter) reference electrode, and a Pt coil (1 mm diameter) counter electrode. Pt was used as the reference electrode material instead of the frequently reported Ag, because iodide anions from the ILs adsorbed on to silver, which lead to destabilization of the reference potential with respect to Ag. A thermally controlled water jacket around the experimental cell maintained the electrolyte temperature. Three-electrode EIS for the GC working electrode was performed using the same cell and the same equipments as those used for CV measurements. These EIS experiments used sine wave perturbations of 10 mV amplitude over a frequency range between 0.1 Hz and 100 kHz. The recorded EIS data were validated by KK transform tests, and then CNLS analyzed to determine EEC models of the experimental interface. The uncertainties in the impedance elements accepted from the CNLS calculations were restricted at < 5%. All the aforementioned measurements were duplicated and the results were repeatable.

3. Results and Discussion

3.1. Synthesis. The one-step halogenation of alcohols using triphenylphosphine and carbon tetrahalide, although quite successful with nonpolar alcohols,[37] is relatively difficult to apply for iodination of mPEG. The separation of polar triphenylphosphine oxide byproduct from the mPEG iodide is tedious. An alternative approach was, therefore, used to obtain the mPEG iodides. The reactions used for the synthesis of the mPEG*n*ImI ILs are shown in Scheme 1.

The tosylation and iodination of PEG were carried out using reported procedures,[38−40] with some modifications. At the end of the tosylation reaction, the crude product was washed with satd. $NaHCO_3$ soln. to remove excess TsCl, and the TsOH formed by hydrolysis. Further washing with aq. HCl soln. ensured complete removal of pyridine. The yield of the tosylation reaction (defined as the moles of mPEG tosylate in the product divided by the moles of mPEG used in the reaction) was about 86% for mPEG7, 72% for mPEG12, and 64% for mPEG16. The yield was calculated using the mass of the crude product and the relative areas of the $Ar-CH_3$ peak at 2.45 ppm and the OCH_3 peak at 3.38 ppm in ^1H NMR spectroscopy.

The crude product contained 6 to 11% of the starting mPEG, and was used in the iodination reaction without further purification. Reaction of the mPEG tosylates with NaI gave mPEG iodides in high yields (> 80%). The product of the iodination reaction was washed with aq. $Na_2S_2O_3$ soln. to remove any iodine that may have formed during the reaction. The quaternization reactions were carried out in DMF at 80 °C. Product yields up to 70% were obtained. The imidazolium salts were insoluble in Et_2O, and could be obtained in high purity after extraction of impurities with this solvent. The unreacted 1-alkylimidazole and mPEG iodide reactants, and the mPEG alcohols originating from incomplete separation in the previous steps, were extracted in to Et_2O and separated from the product. The reaction used in the preparation of the C_nMeImI ILs is shown in Scheme 2. Because of the highly exothermic nature of the

(34) Katayama, Y. In *Electrochemical Aspects of Ionic Liquids*; Ohno, H., Ed.; Wiley: Hoboken, NJ, 2005; Chapter 3.
(35) Zhang, J.; Bond, A. M. *Analyst (Cambridge, U.K.)* **2005**, *130*, 1132.
(36) Aliaga, C.; Baldelli, S. *J. Phys. Chem. B* **2006**, *110*, 18481.
(37) Krishnan, S.; Ward, R. J.; Hexemer, A.; Sohn, K. E.; Lee, K. L.; Angert, E. R.; Fischer, D. A.; Kramer, E. J.; Ober, C. K. *Langmuir* **2006**, *22*, 11255.
(38) Schou, O.; Larsen, P. *Acta Chem. Scand. B* **1981**, *35*, 337.
(39) Dust, J. M.; Fang, Z. H.; Harris, J. M. *Macromolecules* **1990**, *23*, 3742.
(40) Yue, Z; Cowie, J. M. G. *Macromolecules* **2002**, *35*, 6572.

Scheme 1. Synthesis of Methoxy-Terminated PEG Imidazolium Iodides

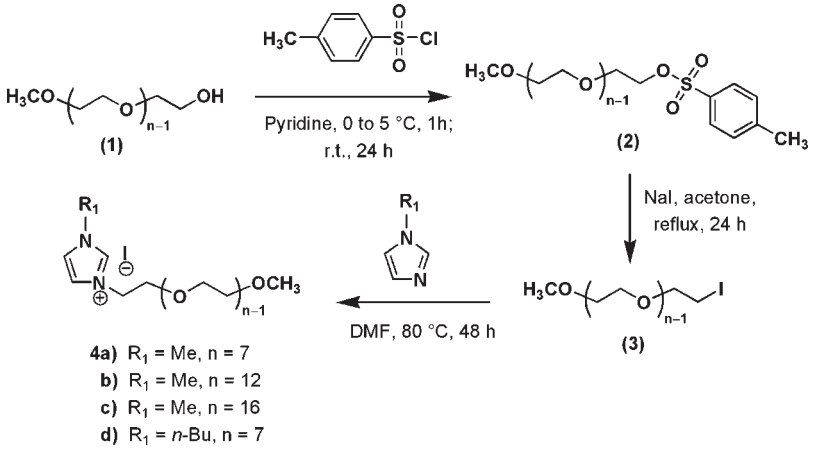

Scheme 2. Synthesis of 1,3-Dialkyl Imidazolium Iodides

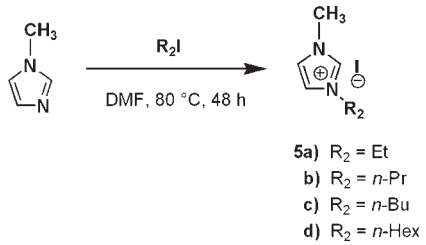

reaction,[41] we expect high theoretical reaction extents. The lower experimental yield, of about 70%, is mainly due to loss during workup and purification. Of the eight Im salts shown in Schemes 1 and 2, only EtMeImI (**5a**, Scheme 2) was a crystalline solid at room temperature. All of the Im salts were dried in a vacuum oven at 50 °C for 24 h before thermal, viscosity, and electrical characterization. The coulometric Karl Fischer method is generally used to determine moisture contents of ILs. However, we are not aware of any reported study which confirms that this method can be applied to iodide containing ILs. Because the working principle of this method is the determination of current required to generate I_2 from I^- ions (generated by the stoichiometric reaction of moisture in the sample with iodine and SO_2),[42] the accuracy of this method, in the case of ILs with iodide anions, does not seem fully warranted. Therefore, for an overall evaluation of moisture effects in the present work, we estimated the water content of mPEG12MeImI IL using ^{1}H NMR spectroscopy (cf. Supporting Information). The moisture in mPEG12-MeImI was found to be about 4300 ppm (0.43 wt %). This amount is higher than moisture content of similarly dried relatively hydrophobic ILs such as BuMeImTf$_2$N (460 ppm) and BuMeImBF$_4$ (1900 ppm), and is comparable to water concentration in more hydrophilic ILs such as 1-*n*-butyl-3-methylimidazolium dicyanamide (5150 ppm).[53]

The influence of the mPEG tails on the electronic structure of the Im ring is evident from the slight upfield shift of the N^+CHN protons of the Im ring in mPEG-derivatized

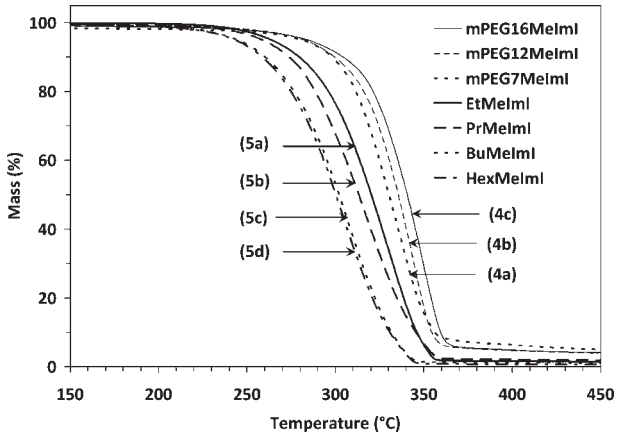

Figure 1. Thermogravimetry plots of the MeImI ILs.

ILs compared to the alkyl-derivatized ionic liquids. The N^+CHN protons in HexMeImI, BuMeImI, PrMeImI and EtMeImI are deshielded to a greater extent than the N^+CHN protons in mPEG*n*MeImI. The N^+CHN proton resonance decreases from about 10.17 ppm in HexMeImI to about 9.78 ppm in mPEG12MeImI. This observation is in good agreement with the NMR spectra of physical blends of BuMeImBF$_4$ and PEG18 reported by Luo et al.,[23] who attributed to the upfield shift of the N^+CHN proton resonance in the PEG-containing blends to the solvation of the Im ring of the IL by the PEG chain.

Although the primary focus of this work was on PEGylated imidazolium iodides, ILs with other anions such as tetrafluoroborate, hexafluorophosphate, trifluoromethanesulfonate, bis(trifluoromethylsulfonyl)imide, acetate, trifluoroacetate, nitrate, isothiocyanate, mesylate, or tosylate, can be synthesized by anion metathesis reaction on the iodide precursors synthesized herein, using free acids, salts of Group 1 metals, ammonium salts, or silver salts.[17,43,44]

3.2. Thermogravimetric Analysis. Figure 1 shows thermogravimetry curves for the mPEG*n*MeImI (**4a**−**c**; cf. Scheme 1), and C$_n$MeImI (**5a**−**d**; cf. Scheme 2) ILs. Table 1

(41) Kabo, G. J.; Paulechka, Y. U.; Kabo, A. G.; Blokhin, A. V. *J. Chem. Thermodynamics* **2010**, *42*, 1292.
(42) Mabrouk, P. A.; Castriotta, K. *J. Chem. Educ.* **2001**, *78*, 1385.
(43) Clare, B.; Sirwardana, A.; MacFarlane, D. R. In *Ionic Liquids*; Kirchner, B., Ed.; Topics in Current Chemistry Series 290; Springer-Verlag: Berlin, 2009; p 1.
(44) Yoshizawa, M.; Ito-Akita, K.; Ohno, H. *Electrochim. Acta* **2000**, *45*, 1617.

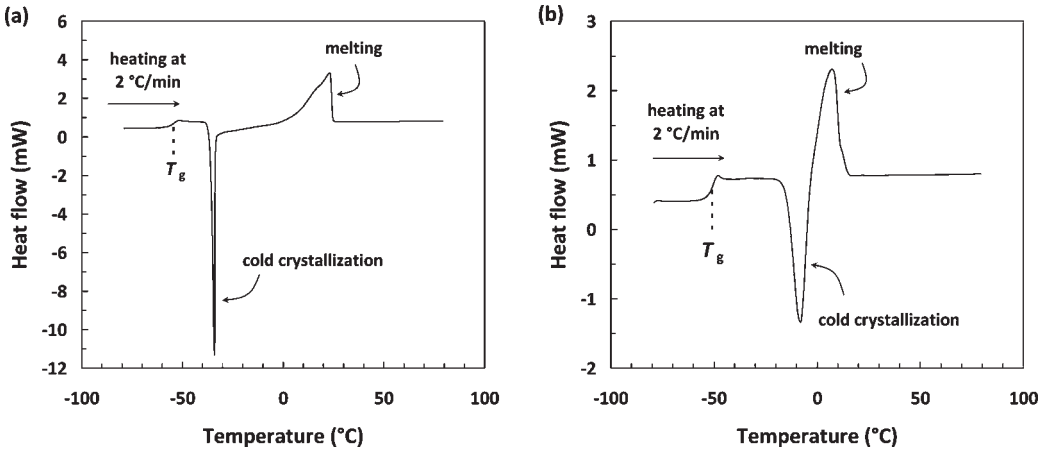

Figure 2. DSC thermograms of (a) mPEG16MeImI and (b) mPEG12MeImI; data obtained during the 2nd heating cycle are shown.

Table 1. Thermal Decomposition Temperatures of MeImI ILs with Different Side Chains

IL	mPEG16	mPEG12	mPEG7	Et	Pr	Bu	Hex
T_d (°C)	284	282	281	264	259	245	243
$T_{d,max}$ (°C)	349	346	331	333	317	306	302

lists the temperature corresponding to 5% mass loss, T_d, and the temperature corresponding to the peak in the rate of mass loss ($-dm(t)/dT$, where m is the mass of sample in the pan at time t, and temperature T).

The data in Figure 1 show that the Im salts are stable up to at least about 200 °C. Mass loss in TGA occurs because of physical volatilization and chemical degradation. The decomposition temperature of C_nMeImI decreases with an increase in alkyl chain length, which we attribute to a decrease in the lattice potential energy of ILs with an increase in the alkyl chain length. The cation−anion interaction energy,[45−47] and therefore the lattice energy,[48] density,[48] and melting point[45,46] decrease with increasing alkyl chain lengths. Thus, HexMeImI shows a greater mass loss at a given temperature than EtMeImI, and the temperature for the onset of mass loss, T_d, of C_nMeImI is lower for the longer *N*-alkyl tails. At temperatures significantly higher than T_d, chemical degradation is the predominant mechanism of mass loss. The dealkylation reaction caused by the nucleophilic I^-,[49−51] results in the formation of relatively volatile uncharged species, the evaporation of which is recorded as a decrease of material mass measured in TGA. The temperature threshold for decomposition of mPEG*n*MeImI ILs is higher than that of C_nMeImI (cf. Figure 1 and Table 1), which can be explained by the stronger intermolecular forces of interaction in the PEGylated ILs at high temperatures (≳ 200 °C). Although Coulombic interactions are shielded to a greater extent by the mPEG tails in **4a**−**c** (than the alkyl tails in **5a**−**d**), there are strong van der Waals (vdW) interactions between the polar mPEG side chains in these ILs. Moreover, the wrapping of mPEG tails around the Im ring[23] is expected to hinder attack of I^- on the Im ring, thereby delaying the onset of chemical degradation. The slight increase in T_d with an increase in the length of the mPEG side chain is attributed to greater vdW interactions between the longer side chains. Interactions between the nonpolar alkyl tails of C_nMeImI, on the other hand, are much weaker than that in the case of mPEG side chains.

3.3. Differential Scanning Calorimetry. Figure 2 shows the DSC thermograms of mPEG16MeImI and mPEG12MeImI. Glass-transition temperatures (T_g) are observed at −54.5 and −50.9 °C for the mPEG16 and mPEG12 ILs, respectively (cf. Figure 2). mPEG7MeImI shows a T_g at −50.5 °C (see the Supporting Information). mPEG16MeImI exhibits a cold crystallization peak, T_{cc}, at −34 °C and a melting peak, T_m, at about 23 °C. The magnitude of the enthalpy change of crystallization or melting is 68 ± 5 J/g (63.1 ± 4.6 kJ/mol). mPEG12MeImI shows a T_{cc} at −8 °C and a T_m at 7 °C. The enthalpy change of these transitions is about 36 ± 3 J/g (27.1 ± 2.3 kJ/mol). Thus, the melting point and the enthalpy of melting increase with an increase in the mPEG chain length, evidently due to intermolecular vdW interactions between the mPEG side chains, as discussed in section 3.2. No crystallization or melting peaks were observed for the salt with the shortest mPEG side chains (**4a** and **4d**), suggesting only weak interactions between mPEG7 side chains. The enthalpy of melting of the PEGylated ILs is notably lower than the enthalpy of melting of 100% crystalline PEG polymer (196.8 J/g),[52] because of the nonlinear (not extended) conformation and relatively amorphous nature of the mPEG chains in these ILs. Using the mass fractions

(45) Turner, E. A.; Pye, C. C.; Singer, R. D. *J. Phys. Chem. A* **2003**, *107*, 2277.
(46) Dong, K.; Zhang, S.; Wang, D.; Yao, X. *J. Phys. Chem. A* **2006**, *110*, 9775.
(47) Tokuda, H.; Hayamizu, K.; Ishii, K.; Susan, Md. A. B. H.; Watanabe, M. *J. Phys. Chem. B* **2005**, *109*, 6103. The weaker interaction has been attributed to the increase in the inductive effect of the alkyl side chains with an increasing *N*-alkyl chain length, which reduces the positive charge on the imidazolium cation by charge delocalization.
(48) Glasser, L. *Thermochim. Acta* **2004**, *421*, 87.
(49) Chan, B. K. M.; Chang, N.-H.; Grimmett, M. R. *Aust. J. Chem.* **1977**, *30*, 2005.
(50) Ngo, H. L.; LeCompte, K.; Hargens, L; McEwen, A. B. *Thermochim. Acta* **2000**, *357*−*358*, 97.
(51) Huddleston, J. G.; Visser, A. E.; Reichert, W. M.; Willauer, H. D.; Broker, G. A.; Rogers, R. D. *Green Chem.* **2001**, *3*, 156.
(52) Pielichowski, K.; Flejtuch, K. *Polym. Adv. Technol.* **2002**, *13*, 690.

Table 2. Densities of MeImI ILs at 25 °C

IL	mPEG16	mPEG12	mPEG7	Hex	Bu	Pr
ρ_L (g/cm^3)	1.262 ± 0.003	1.294 ± 0.023	1.363 ± 0.004	1.408 ± 0.021	1.519 ± 0.009	1.553 ± 0.020

of the mPEG side chains in the ILs, the experimentally determined enthalpies of melting, and the enthalpy of melting of 100% crystalline PEG, the percent crystallinity of the mPEG tails in mPEG16MeImI, mPEG12MeImI, and mPEG7MeImI is estimated to be about 45, 25, and 0%, respectively. The degree of crystallinity of the PEG side chains in the ILs is lower than that of a pure PEG oligomer with a degree of polymerization of 22 (ca. 86% crystallinity).[52]

In cold crystallization, a subcooled liquid crystallizes upon heating above the T_g, and the crystallized sample melts at the melting temperature, T_m, upon further heating. Cold crystallization of BuMeIm ILs with hexafluorophosphate (PF_6) (−37 °C), Tf_2N (−44 °C), and dicyanamide (−29 °C) anions,[53] BuMeIm IL with bromide anion,[54] and 1-[2-(2-methoxyethoxy)ethyl]-3-methylimidazolium IL with PF_6 anion[55] have been reported in the literature. In contrast, BuMeImI showed a behavior similar to BuMeImBr and BuMeImCl studied by Fredlake et al.,[53] and did not undergo cold crystallization in our experiments. Cold crystallization is influenced by the potential energy of intermolecular interactions and the ability of the molecules to undergo rapid temperature-dependent conformational changes. Because of its stronger intermolecular interactions and lower conformational entropy, mPEG16MeImI has a lower T_{cc} than mPEG12MeImI.

The DSC thermogram of EtMeImI is shown in the Supporting Information. An exothermic melting peak at 81.5 °C appears during heating. The EtMeImI melting point of 81.5 °C is in good agreement with the value of 78 °C reported by Every et al.[56] The enthalpy of melting, 74 ± 7 J/g (17.6 ± 1.7 kJ/mol), is in reasonable agreement with the value of 16.5 kJ/mol reported by Turner et al.[45] A sharp endothermic crystallization transition occurs at 15 °C during cooling. Thus, EtMeImI is capable of existing as a supercooled liquid up to a temperature of 15 °C, when its melt is rapidly cooled. In contrast to the ionic liquids with long mPEG tails, none of the C_nMeImI ILs showed a cold crystallization peak.

3.4. Liquid Density. Both mPEG*n*MeImI and C_nMeImI were liquids at room temperature, and their densities, at 25 °C, are shown in Table 2. The reported values are averages of 5 measurements, and the standard deviation is given as the uncertainty in Table 2. It is seen that for both sets of ILs the density decreases with an increase in the side chain length. These observations are consistent with a previous report on the effect of alkyl chain length on the density of ILs that contained the Tf_2N anion.[53] The lower densities of mPEG*n*MeImI than C_nMeImI is due to weaker intermolecular interactions of the relatively large mPEG*n*-MeIm cations in the PEGylated ILs.

Huddleston et al. have determined the room-temperature densities of BuMeImI, BuMeImCl, BuMeImBF_4, BuMeImPF_6, and BuMeImTf_2N to be 1.44, 1.08, 1.12, 1.36, and 1.43 g/cm^3, respectively.[51] The data of Huddleston et al. indicate that the density of BuMeImI is higher than the densities of BuMeIm ILs with Cl, BF_4, PF_6, and Tf_2N anions. A similar study of the effect of anion on the density of ILs containing the common cation, BuMeIm, has been reported by Fredlake et al.[53] However, densities of the BuMeIm ILs do not show the expected[53] monotonic increase with an increase in the molecular weight of the anion. The molecular weights of the anions increase in the order Cl < BF_4 < I < PF_6 < Tf_2N (35.5, 86.8, 126.9, 144.96, and 280.15 g/mol, respectively). However, the room temperature density increases in the order Cl < BF_4 < PF_6 < Tf_2N < I. The densities do not show a simple correlation to the sizes of the anions either, which increase in the order Cl < I ≈ BF_4 < PF_6 (0.047, 0.072, 0.073, and 0.109 nm^3, respectively[57]). Although the effect of anions on the properties of the mPEG*n*MeIm and C_nMeImI needs further investigation, the relatively high densities of the C_nMeImI ILs reported in Table 2 are in very good agreement with the literature values of 1.38 g/cm^3 for HexMeImI, 1.49 g/cm^3 for BuMeImI, and 1.55 g/cm^3 for PrMeImI.[58] Because EtMeImI is a crystalline solid at room temperature, its density could not be measured using our procedure, but its density at 80 °C has been estimated to be 1.69 g/cm^3.[56]

3.5. Temperature and Shear Rate Dependence on Shear Viscosity. Temperature-dependent viscosities of the ILs were determined starting at 95 °C and decreasing the temperature in steps of 5 °C down to 20 °C. The viscosity of EtMeImI could be determined only at temperatures ≥40 °C. The fluidity was too low below this temperature to allow viscosity determination using our instrument. All of the ILs, including EtMeImI and mPEG16MeImI, show a Newtonian behavior in the temperature range of measurements. Tables of viscosities of the ionic liquids at different temperatures are given in the Supporting Information. The room temperature viscosities of C_nMeImI ILs, determined in this work, are in good accord with the values reported by Kubo et al.[32] Figure 3a shows the viscosity of the ionic liquids in the temperature range of 60 to 95 °C.

The viscosities of the mPEG*n*MeImI ILs are lower than those of HexMeImI. For both mPEG*n*ImI and C_nMeImI, the viscosity increases with an increase in the length of the side chains. The effect is more pronounced in the case of alkyl-derivatized ILs than in the case of mPEG-derivatized ILs. The increase in viscosity of C_nMeImI with an increase

(53) Fredlake, C. P.; Crosthwaite, J. M.; Hert, D. G.; Aki, S. N. V. K.; Brennecke, J. F. *J. Chem. Eng. Data* **2004**, *49*, 954.
(54) Nishikawa, K.; Wang, S.; Katayanagi, H.; Hayashi, S.; Hamaguchi, H.; Koga, Y.; Tozaki, K. *J. Phys. Chem. B* **2007**, *111*, 4894.
(55) Diogo, H. P.; Ramos, J. J. M. *Phase Transitions* **2005**, *78*, 357.
(56) Every, H. A.; Bishop, A. G.; MacFarlane, D. R.; Orädd, G.; Forsyth, M. *Phys. Chem. Chem. Phys.* **2004**, *6*, 1758.
(57) Jenkins, H. D.; Roobottom, H. K.; Passmore, J.; Glasser, L. *Inorg. Chem.* **1999**, *38*, 3609.
(58) Cao, Y.; Zhang, J.; Bai, Y.; Li, R.; Zakeeruddin, S. M.; Grätzel, M.; Wang, P. *J. Phys. Chem. C* **2008**, *112*, 13775.

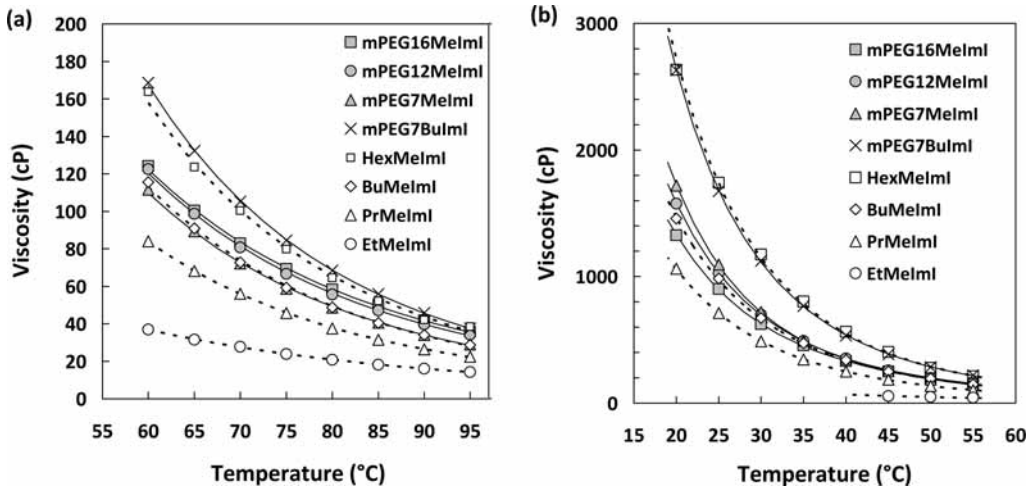

Figure 3. Temperature dependence of shear viscosity, η, of the ionic liquids over the temperature range of (a) 60−95 °C, and (b) 20−55 °C. The open symbols correspond to experimental data for the 1-alkyl-3-methylimidazolium iodides, whereas the filled symbols correspond to the mPEG imidazolium iodides. The curves represent fit of experimental data to an Arrhenius equation for the range of higher temperatures and VFT equation for the range of lower temperatures.

in the alkyl chain length is in agreement with prior reports.[56,59]

The effect of ether oxygen atoms in lowering the viscosity is clearly evident. BuMeImI has 4 atoms along the side chain backbone, while mPEG7MeImI has 22 atoms in the mPEG backbone. The viscosities of the two ILs are, however, similar. Likewise, even though mPEG16MeImI has 49 atoms in the side chain backbone, its viscosity is lower than that of HexMeImI, which has only 6 carbon atoms in the backbone. mPEG7BuImI, with the bulky *n*-butyl group attached to the ring nitrogen, has a significantly higher viscosity than its homologue, mPEG7MeImI, wherein the nitrogen atom is attached to a methyl group instead. Nevertheless, the viscosity of mPEG7BuImI is only slightly higher than that of HexMeImI. In all the mPEG-functionalized ILs, the mPEG side chain serves to screen Coulombic interactions between the Im ring and the iodide anion, thereby lowering the viscosity. Shirota and Castner have observed a similar fluidity increase with silicon-substituted imidazolium ILs.[60,61] The viscosities of trimethylsilylmethyl-derivatized methylimidazolium ILs (with Tf_2N and BF_4 anions) were found to be significantly lower than ILs that contained the isostructural neopentyl group in the cation. Si−C bond lengths are substantially longer than C−C bond lengths. Hence, the volume of the trimethylsilylmethyl-substituted cation is higher than that of the neopentyl-derivatized cation.[60] Because of the larger cation size, intermolecular interactions between a given anion and the silicon-derivatized cation are weaker, leading to lower viscosity.

The high temperature viscosity values conform quite well to the Arrhenius equation, $\eta = \eta_0 \exp(E_a/RT)$, where η_0 is the limiting viscosity, E_a the activation energy, R the gas constant, and T the absolute temperature. The relaxation times of molecules in liquids, and hence the liquid viscosity, can be expected to show Arrhenius dependence on temperature, at relatively high temperatures. At lower temperatures the Vogel−Fulcher equation, which is based on the Adam−Gibbs equation that relates the relaxation time to the configurational entropy of the system,[62] usually gives a better fit to the experimental data. According to the theory of viscosity of liquids developed by Eyring et al.,[63] the temperature dependence of liquid viscosity is approximately of the Arrhenius form, $\eta = (h/\upsilon) \exp(\Delta G_0/RT)$ where h is the Planck constant, υ is the volume of a single particle (molecule, or a micellar aggregate) of fluid, and ΔG_0 is the molar free energy of activation, for the escape of the fluid particle from its "cage," in the stationary fluid. For a simple fluid, $\upsilon \approx V_L/N_A$ where V_L is the liquid molar volume and N_A is the Avogadro number.

The activation energies, E_a ($\equiv \Delta G_0$), listed in Table 3 show different trends for the mPEG*n*ImI and C_nMeImI. For the mPEG*n*MeImI ILs, the activation energy, E_a, decreases slightly with an increase in the length of mPEG group. For the C_nMeImI ILs, on the other hand, E_a increases significantly with an increase in the length of the alkyl side chain. The weaker dependence of E_a on mPEG tail length is another indication of the nonlinear conformation of the mPEG tails (cf. section 3.3).

For "normal" liquids, the activation energy for viscous flow is proportional to the potential energy of intermolecular interactions.[64,65] However, this result may be extended to the ILs of the present study only with caution. Although

(59) Bai, Y.; Cao, Y.; Zhang, J.; Wang, M.; Li, R.; Wang, P.; Zakeeruddin, S. M.; Grätzel, M. *Nat. Mater.* **2008**, *7*, 626.
(60) Shirota, H.; Castner, E. W., Jr. *J. Phys. Chem. B* **2005**, *109*, 21576.
(61) Chung, S. H.; Lopato, R.; Greenbaum, S. G.; Shirota, H.; Castner, E. W., Jr.; Wishart, J. F. *J. Phys. Chem. B* **2007**, *111*, 4885.
(62) Angell, C. A. *J. Phys. Chem.* **1966**, *70*, 2793.
(63) Bird, R. B.; Stewart, W. E.; Lightfoot, E. N. *Transport Phenomena*; Wiley: New York, 1994; Chapter 1, and the references therein.
(64) Kincaid, J. F.; Eyring, H.; Stearn, A. E. *Chem. Rev.* **1941**, *28*, 301. Kincaid et al. defined normal liquids as those in which the forces between molecules are undirected, as in carbon tetrachloride or benzene, or liquids in which intermolecular forces were directed in part, as in ethyl chloride, ethyl bromide, acetone, or *para*-nitrobenzene. The dipole-containing molecules exhibit weak association in pairs, or form a two- or three-dimensional network of dipole bonds. Hydrogen-bonded liquids and molten salts were not considered simple fluids and showed large deviations in the linear correlation between activation energy of viscosity, ΔG_0, and heat of vaporization, ΔU_{vap}. Furthermore, the proportionality between ΔG_0 and ΔU_{vap} is not valid for molecules with high aspect ratio, e.g., long slender molecules such as higher alkanes.
(65) Moganty, S. S.; Baltus, R. E. *Ind. Eng. Chem. Res.* **2010**, *49*, 5846.

Table 3. Temperature Dependence of Viscosity of Ionic Liquids in the Temperature Range of 60−95 °C[a]

ionic liquid	$\eta_0 \times 10^4$ (cP)	E_a (kJ/mol)	r^2
mPEG16MeImI	2.750	36.02	0.9996
mPEG12MeImI	1.800	37.15	0.9993
mPEG7MeImI	0.757	39.30	0.9993
mPEG7BuImI	0.249	43.54	0.9999
HexMeImI	0.279	43.07	0.9955
BuMeImI	0.512	40.45	0.9991
PrMeImI	0.722	38.68	0.9998
EtMeImI	16.22	27.78	0.9997

[a] $\eta = \eta_0 \exp(E_a/RT)$; r is the Pearson product-moment correlation coefficient for the linear fit of ln η vs $1/T$.

intermolecular forces are expected to be weaker in the 1,3-dialkylimidazolium iodides with longer alkyl tails,[45,46,48] their viscosity activation energies are higher (cf. Table 3). Nevertheless, the E_a values reported in Table 3 are lower for the mPEG*n*MeImI ILs than HexMeImI or BuMeImI.

In the case of C_nMeImI, the increase in the activation energy with an increase in the alkyl chain length is consistent with the behavior of molten metal carboxylate surfactants reported by Ekpe and Sime.[66] The formation of micelle-like aggregates in HexMeImI is expected to be a reason for this observation. This reasoning is in accord with prior reports that Im ILs with side chains longer than C_3 are microstructured in the fluid phase, wherein the nonpolar alkyl chains form microdomains that are distinct from ionic domains formed by the Im ring and the anion.[67,68] The values of limiting viscosity, η_0, shown in Table 3 were also found to vary with the length of the side chains and, based on the Eyring theory, are expected to be inversely proportional to the volume occupied by the fluid particle.

Figure 3b shows the viscosity of the ILs in the temperature range of 20 to 55 °C. Similar to the viscosity behavior at higher temperatures (cf. Figure 3a), the lower temperature viscosities of the alkyl-derivatized ILs in Figure 3b also exhibit a strong dependence on the alky chain length (2, 3, 4, or 6 carbon atoms). The viscosities of the mPEG*n*MeImI ILs show a weaker dependence on side chain length (22, 37, or 49 atoms along the backbone). Although the side chains are significantly longer in the mPEG*n*MeImI ILs, their viscosities are lower than those of HexMeImI. The activation energy for viscous flow at temperatures between 20 and 55 °C, calculated using the Eyring theory, are shown in the Supporting Information. The E_a values are higher than those reported in Table 3, but show similar trends in variations with the side chain length. In this range of temperatures, the viscosity of mPEG16MeImI is lower than those of mPEG12-MeImI and mPEG7MeImI. We attribute this behavior primarily to the formation of molecular aggregates of mPEG16MeImI with larger fluid particle volume, v, at lower temperatures. The effect of the mPEG chains in lowering the viscosity is clearly evident when the molecular weight normalized viscosities are compared, in the form of the Orrick and Erbar viscosity plots, as shown in the Supporting Information. Additional mechanisms could also contribute to promoting different correlations between the temperature dependent trends and the molecular sizes of the ILs in the two temperature segments explored in panels a and b in Figure 3. For instance, these effects could arise from a temperature -sensitive competition between Coulombic and vdW forces that dictate the IL viscosities.[69]

3.6. Ionic Conductivity. Figure 4 shows conductivities of the mPEG*n*ImI and C_nMeImI ILs, measured using EIS, and displayed on logarithmic ordinates.

In the 60−95 °C temperature range, the specific conductivities of all the ILs tested in Figure 4a follow the Arrhenius equation, $\lambda = \lambda_0 \exp(-E_a'/RT)$, with E_a' and λ_0 representing the activation energy of conductivity and the limiting conductivity, respectively. The activation energy for ionic conductivity, and the VFT fit parameters for the λ vs T data are given in the Supporting Information. The activation energy for conductivity, E_a', and the activation energy for viscosity, E_a, show similar trends for C_nMeImI with variation in the length of the alkyl tail. In the case of mPEG*n*ImI ILs, E_a' shows a weaker dependence on the mPEG chain length.

In the temperature window of Figure 4a, $\lambda(T)$ for mPEG*n*MeImI ILs decreases with increasing lengths of the mPEG side chains, and the same behavior continues at lower temperatures in Figure 4b, up to ca. 30 °C. At temperatures below about 30 °C, however, mPEG16MeImI has higher conductivities than those of mPEG7MeImI and mPEG12MeImI. This reversal of trend in $\lambda(T)$ below 30 °C can be linked to the similar molecule-dependent behavior of $\eta(T)$ observed by comparing the viscosity results of Figure 3. Therefore, the factors that govern the relative temperature dependencies of both λ and η of the mPEG*n*MeImI ILs most likely have a common origin. As noted in the context of Figure 3, the underlying mechanisms of these specific effects can be associated with the competitive strengths of Coulombic and vdW interactions at different temperatures, as well as with possible formation of molecular aggregates below 30 °C.

The effect of crystallization on ionic conductivity is clearly evident from the data in Figure 4c. In the temperature range of 60 to 95 °C (Figure 4a), the conductivity of C_nMeImI decreases with an increase in the length of the alkyl tail. EtMeImI has the highest conductivity and HexMeImI has the lowest conductivity among the C_nMeImI ILs. However, below 55 °C, there is a sharp decrease in the conductivity of EtMeImI, even below the conductivities of mPEG*n*MeImI ILs. During conductivity measurement, EtMeImI crystallizes at a temperature between 55 and 50 °C.[70] Ionic conductivity of solid

(66) Ekpe, U. J.; Sime, S. J. *J. Chem. Soc., Faraday Trans. 1* **1976**, *72*, 1144.
(67) Russina, O.; Triolo, A.; Gontrani, L.; Caminiti, R.; Xiao, D.; Hines, L. G., Jr.; Bartsch, R. A.; Quitevis, E. L.; Plechkova, N.; Seddon, K. R. *J. Phys.: Condens. Matter* **2009**, *21*, 424121.
(68) Jacquemin, J.; Husson, P.; Padua, A. A. H.; Majer, V. *Green Chem.* **2006**, *8*, 172.
(69) Tokuda, H.; Tsuzuki, S.; Susan, Md. A. B. H.; Hayamizu, K.; Watanabe, M. *J. Phys. Chem. B* **2006**, *110*, 19593.
(70) Although the melting temperature of EtMeImI is 81.5 °C (cf. section 3.3), it can exist as supercooled liquid up to a significantly lower temperature. The crystallization temperature is lower when the IL is cooled at a faster rate. Hence, a higher crystallization temperature, between 50 and 55 °C, is observed in the conductivity experiments than in the DSC experiment (15 °C) where the cooling rate was faster.

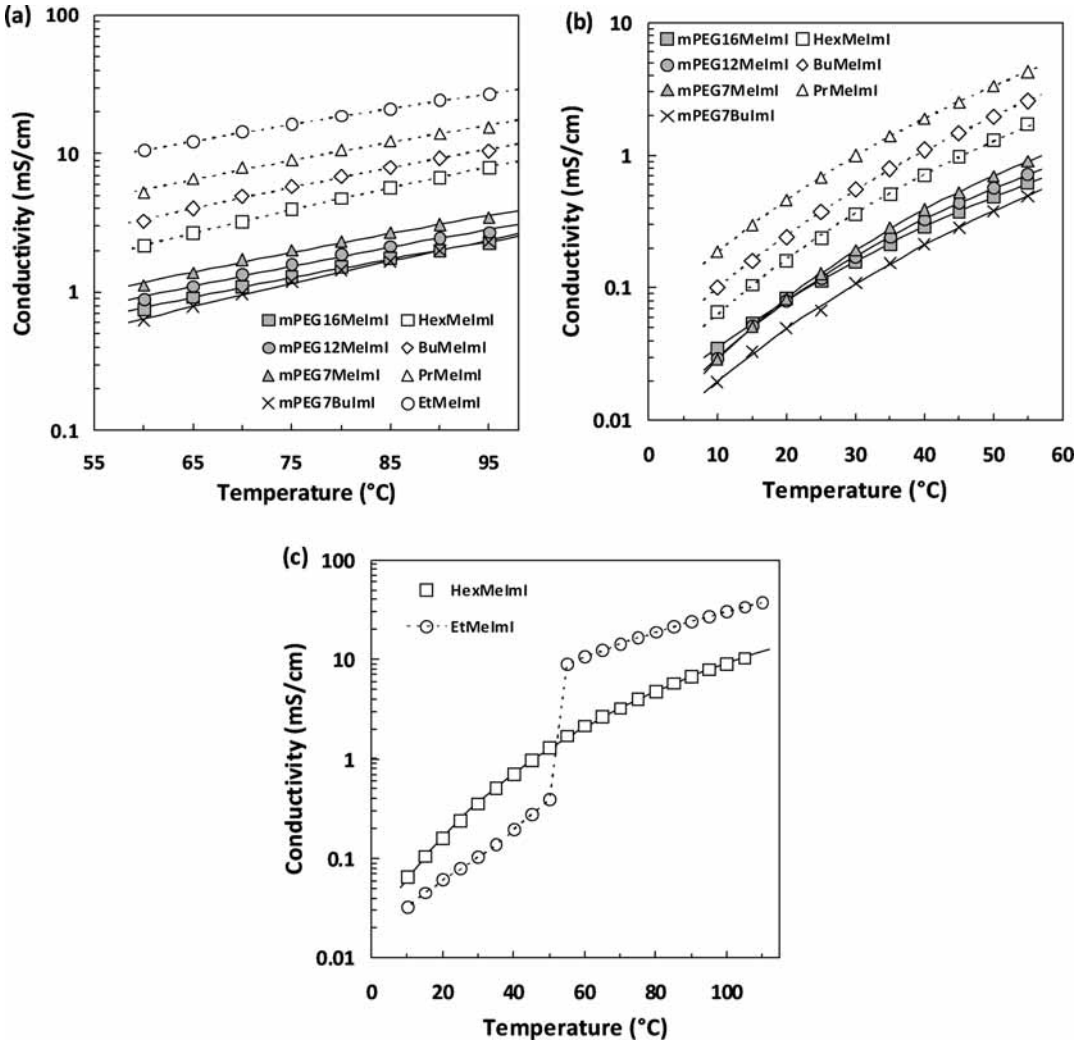

Figure 4. Temperature dependence of IL conductivities. The curves represent fit of experimental data to (a) Arrhenius equation or (b) VFT equation. (c) Conductivity data for HexMeImI and EtMeImI are compared to show the effect of crystallization on ionic conductivity.

EtMeImI is about 2 orders of magnitude lower than that of liquid EtMeImI. Unlike the behavior of EtMeImI that shows a discontinuous conductivity drop between 50 and 55 °C, all of the mPEG*n*ImI ILs show a continuous decrease in conductivity with a decrease in temperature.

In Figure 5, the conductivities of the ILs are plotted against their viscosities, where two distinct groups of data can be identified for the two types of ILs. At each viscosity value, the conductivity of mPEG*n*MeImI is ca. 4-fold lower than that of C$_n$MeImI. The difference in the conductivity values is caused by the different ionic concentrations of the two sets of ILs. Because of the relatively high molecular weights of the polymeric PEGylated ILs, the concentration of ions in these ILs is lower.

Based on the Nernst−Einstein and Stokes−Einstein equations, the correlation between λ and η can be expressed as[17]

$$\log(\lambda) = \log\left[\frac{yF^2\rho_L}{6\pi N_A M}\left(\frac{1}{\xi_a R_a}+\frac{1}{\xi_c R_c}\right)\right] - \log(\eta) \quad (1)$$

where y is the degree of dissociation, F is the Faraday constant, ρ_L is the IL density, N_A is the Avogadro constant, M is the molar mass of the IL, ξ_a and ξ_c are correction factors that account for specific interactions between the mobile ions in the melt, and R_a and R_c are the radii of the anion and cation, respectively. Within each group of ILs in Figure 5, the slopes of the conductivity vs viscosity data,

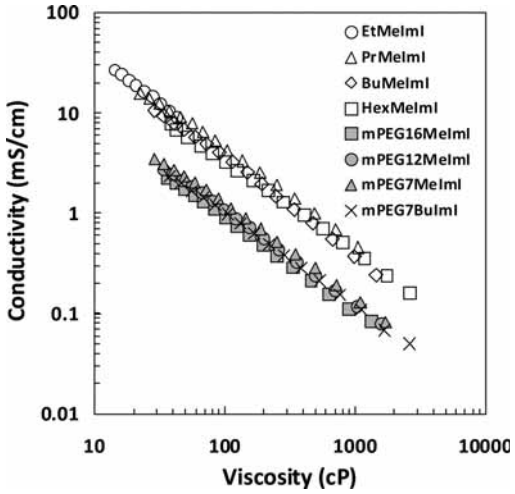

Figure 5. Conductivity versus viscosity of mPEG- and alkyl-derivatized ILs, at different temperatures.

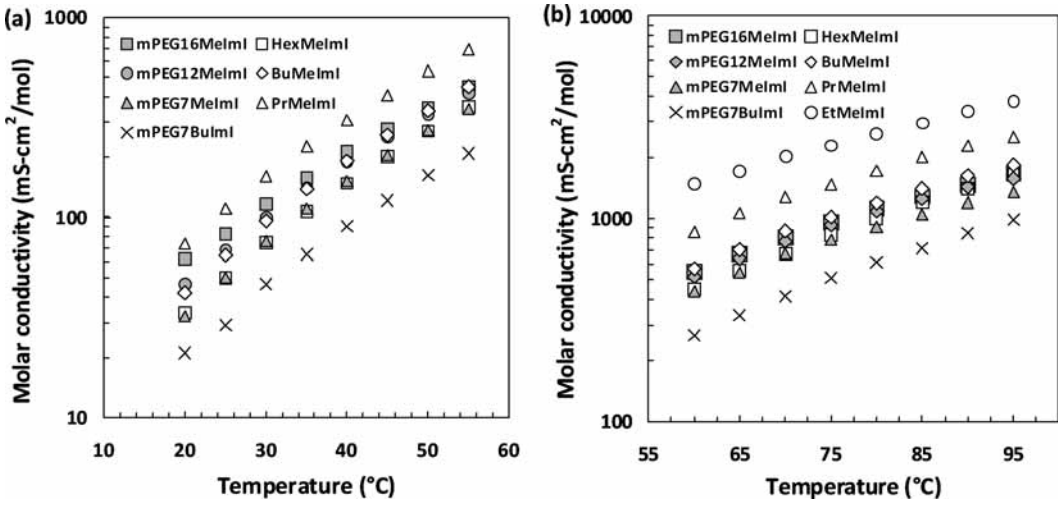

Figure 6. Molar conductivity of the ILs at different temperatures.

which are linear on a log−log scale, are relatively insensitive to the molar masses or radii of the cations. On the other hand, the intercept of the linear $\log(\lambda)$ versus $\log(\eta)$ graph is higher for the C_nMeImI ILs, and these samples have lower molar mass and cation radii between the two groups of ILs compared. The observations of Figure 5 are consistent with the description of eq 1.

The effect of the concentration of charge carriers on conductivity can be characterized using molar conductivity, which is the ratio of conductivity and molar concentration of the ILs. Figure 6 shows the molar conductivity, Λ, of the ILs calculated using $\Lambda = \lambda M/\rho_L$. Room-temperature density (Table 2) is used to calculate the molar conductivities. In the case of the C_nMeImI ILs, molar conductivity decreases with an increase in the length of the alkyl side chain, as expected. In contrast, among the mPEG*n*ImI ILs, the molar conductivity is higher for mPEG16MeImI that has a longer mPEG side chain. The interaction between the Im cation and the iodide anion is expected to be the weakest for this IL. Its molar conductivity is, therefore, higher than those for the other mPEG*n*ImI ILs. Molar conductivity of mPEG7BuImI is the lowest among the set of samples studied here. Replacing the methyl group in mPEG7MeImI with the longer *n*-butyl group significantly lowers molar conductivity at all temperatures.

Figure 7 shows a plot of molar conductivity versus viscosity for the eight ILs at different temperatures between 20 and 95 °C. The data points for both sets of ILs now cluster near a single curve, represented by the solid line through the symbols. The parameters used for this line-fit are indicated in the figure. It is seen from this plot that $\Lambda \propto \eta^{-0.94}$, or in other words, the product, $\Lambda\eta^{0.94}$, is a temperature-independent constant. The observed value, 0.94, of the exponent is close to the value of 1.00 expected from the equation, $\Lambda\eta = [yF^2/(6\pi N_A)][(\xi_a R_a)^{-1} + (\xi_c R_c)^{-1}]$, based on eq 1, and is in very good agreement with the value of 0.90−0.94 for fluoroborate-based ILs, recently reported by Schreiner et al.[71]

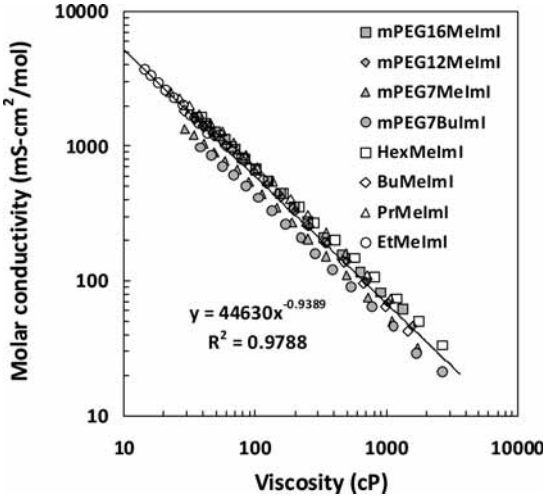

Figure 7. Viscosity dependence of molar conductivity of the ILs.

3.7. Electrochemical Window. Because of the incorporation of the faradaically active I^- in the ILs synthesized here, they are somewhat different from the electrolytes generally encountered in conventional evaluation of strictly nonfaradaic electrochemical windows. However, although a redox-active voltage segment is indeed expected for these ILs, they should also support a reasonably wide nonfaradaic voltage region outside the redox region, to meet the overall criterion of electrochemical stability. As electrolytes for DSSCs, this latter feature of the ILs is essential for adequately supporting the standard current−voltage characterization tests of such devices, where the bias cell voltage is varied over a certain range to selectively promote the I^-/I_3^- redox process without allowing other side reactions.[72] Such nonfaradaic voltage regions are also necessary to utilize these electrolytes in supercapacitors and certain types of sensors.[73] On the basis of these considerations, tests of temperature-dependent electrochemical

(71) Schreiner, C.; Zugmann, S.; Hartl, R.; Gores, H. J. *J. Chem. Eng. Data* **2010**, *55*, 4372.

(72) Berginc, M.; Krašovec, U. O.; Jankovec, M.; Topič, M. *Sol. Energy Mater. Sol. Cells* **2007**, *91*, 821.

(73) Zheng, J. P; Goonetilleke, P. C.; Pettit, C. M.; Roy, D. *Talanta* **2010**, *81*, 1045.

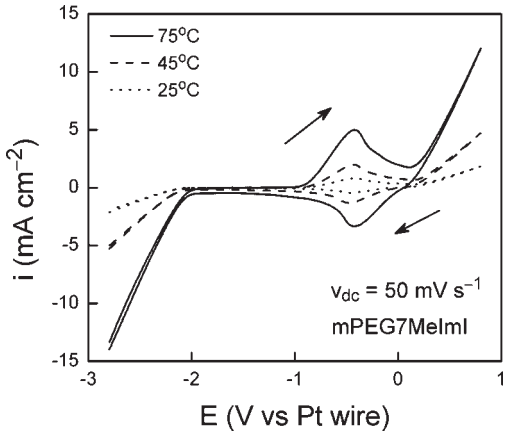

Figure 8. Cyclic voltammograms of mPEG7MeImI at different temperatures.

windows were performed using a representative sample of the PEGylated ILs reported here.

Electrochemical windows of ILs are generally determined using GC or Pt working electrodes.[73] GC provides a large overpotential for the reduction of H^+, whereas on Pt, this reaction is supported at lower overpotentials.[74] In addition, because of its lower work function (4.5 eV) than Pt (5.0 eV), GC tends to be relatively more sensitive toward the intrinsic oxidation/reduction of the constituent ions of the IL electrolyte used.[75] Thus, while Pt serves as an efficient electrode for characterizing the role of residual water in narrowing the electrochemical window of ILs, GC is useful for determining the faradaic voltage limits of the IL's constituent ions. The latter criterion was a primary consideration in the present investigation. Therefore, electrochemical windows were measured here on GC so that even if water impurity were present, its faradaic interference would be minimized.

The mPEG*n*MeImI ILs with longer mPEG side chains showed rather large resistances at room temperature, and would result in large ohmic drop during cyclic voltammetry because of solution resistance.[76] Therefore, for quantitative analysis, only mPEG7MeImI, the IL with the highest conductivity in the set, was investigated with CV using a GC working electrode. Voltammograms obtained for this system at a scan rate of 50 mV s^{-1}, with cell temperatures maintained at 25, 45, and 75 °C, are shown in Figure 8.

The voltammogram recorded at 25 °C is quite similar to the room-temperature data for iodide-containing ILs reported by Zistler et al.[77] Consistent with this earlier report, the expected features of the I^-/I_3^- redox couple appear here in the form of the faradaic currents detected between 0 and −1 V. In our experiments, the I_3^- is formed in situ via oxidation of the I^- anion of the IL. To confirm that the peaklike signature behavior of redox reactions (cf. Figure 8) is associated with the I^-/I_3^- species, we conducted CV experiments using a solution of LiI in an iodide-free imidazolium IL, $EtMeImEtSO_4$. These experiments are discussed in the Supporting Information.

Compared to C_nMeIm salts such as BuMeImBr and EtMeImF reported previously,[78,79] mPEG7MeImI shows a higher resistance against cathodic reduction, as evident from its broad negative range of electrochemical stability observed in Figure 8. The improved stability is attributed to the H-bonding interactions of the mPEG tail with the imidazolium ring. Unlike other Im salts such as $EtMeImEtSO_4$,[73] and $BuMeImBF_4$,[75] the mPEG7MeImI IL at the GC electrode surface appears to be a quasi-reversible system for both the cation, $mPEG7MIm^+$, and the anion, I^-. In addition, the electrochemical window (extending from −1.0 to −2.0 V) of mPEG7MeImI is fairly independent of temperature, as seen in Figure 8.

3.8. Impedance Characteristics and Polarization Resistance. Carbon-based electrodes (such as those used in electrochemical capacitors and similar devices) often contain reactive surface species and impurities.[80] When combined with these electrodes, the experimental electrolyte should be faradaically inert toward these reactants in order to support proper functioning of the device.[81,82] Although the electrochemical window provides the nonreactive voltage range of such an interface, the passivity of the system with respect to charge transfer can be quantified in terms of the polarization resistance, R_p. This resistance was measured for the GC−mPEG7MeIm system using EIS in a three-electrode configuration at the open circuit potentials (OCPs) for different temperatures. Illustrative Nyquist plots from these experiments are presented in Figure 9a, where the OCPs were recorded to be −2, −5, and −5 mV (vs Pt wire), at 25, 45, and 75 °C, respectively.

The symbols in Figure 9a denote experimental EIS data and the lines are CNLS fits to the data using the EEC shown in the inset. This EEC, that includes R_p, is commonly used to describe IL−electrode interfaces,[73] where R_u and Q_{dl} represent the uncompensated solution resistance and the constant phase element (CPE) of the GC working electrode, respectively. The total complex impedance, Z of the system has the form $Z = R_u + R_p[1 + R_p Y_0(j\omega)^n]^{-1}$ where Y_0 is the frequency independent admittance parameter of the CPE, n is the CPE exponent, and $j = (-1)^{1/2}$. As expected in terms of thermal activation of reaction steps, both Z' and Z'' (the real and imaginary components of Z) decrease with increasing temperatures.

Figure 9b displays Z' and Z'' values obtained by KK transform of the Z'' and Z' data from Figure 9a, respectively. The inset in Figure 9b shows a close-up of the high-frequency results. Each KK-transformed Nyquist plot

(74) Mantz, R. A. In *Ionic Liquids in Synthesis*; Wasserscheid, P.; Welton, T. Eds.; Wiley-VCH: Weinheim, 2008; Vol. *1*, p. 141.
(75) Moganty, S. S.; Baltus, R. E.; Roy, D. *Chem. Phys. Lett.* **2009**, *483*, 90.
(76) Bard, A. J.; Faulkner, L. R. In *Electrochemical Methods: Fundamentals and Applications*, 2nd edn.; Wiley: New York, 2001; p. 25.
(77) Zistler, M.; Schreiner, C.; Wachter, P.; Wasserscheid, P.; Gerhard, D.; Gores, H. J. *Int. J. Electrochem. Sci.* **2008**, *3*, 236.
(78) Hagiwara, R.; Hirashige, T.; Tsuda, T.; Ito, Y. *J. Fluorine Chem.* **1999**, *99*, 1.
(79) Lewandowski, A.; Stepniak, I. *Phys. Chem. Chem. Phys.* **2003**, *5*, 4215.
(80) Ranganathan, S.; Kuo, T.-C.; McCreery, R. L. *Anal. Chem.* **1999**, *71*, 3574.
(81) Hashmi, S. A.; Latham, R. J.; Linford, R. G.; Schlindwein, W. S. *J. Chem. Soc. Faraday Trans.* **1997**, *93*, 4177.
(82) Silva, F.; Gomes, C.; Figueiredo, M.; Costa, R.; Martins, A.; Pereira, C. M. *J. Electroanal. Chem.* **2008**, *622*, 153.

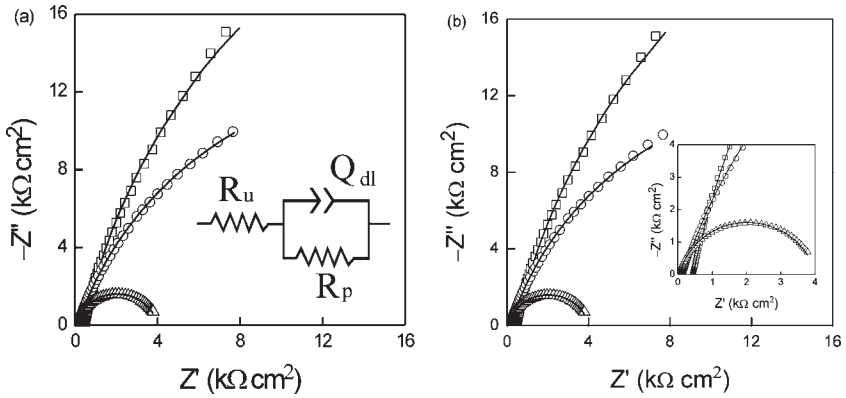

Figure 9. (a) Illustrative Nyquist plot of mPEG7MeImI, measured using a GC working electrode in a three-electrode cell at 25 °C (□), 45 °C (○), and 75 °C (△). The inset in panel a shows the EEC used to CNLS-fit (lines) the experimental data (symbols). (b) KK-transformed version of the full set of data presented in panel a.

in Figure 9b is identical to its original counterpart in Figure 9a, confirming the validity of the EIS data. CNLS fits to the graphs in Figure 9b also lead to the same EEC shown in Figure 9a, resulting in the same set of impedance elements in both cases. These impedance parameters, listed in the order of their values at 25, 45, and 75 °C are as follows: R_p = 64.6, 34.0, and 4.0 Ω cm^2; R_u = 450, 139, and 47 Ω cm^2; and n = 0.88, 0.81, and 0.87. Because the activation barrier against polarization induced charge transfer is lowered at high temperatures, R_p decreases with increasing temperatures. Nevertheless, all the aforementioned values of R_p are relatively large, and represent strongly nonfaradaic nature of the IL-GC interface at equilibrium. For CPEs associated with electrochemical double layers, n can vary between 0 and 1, but for stable solid−liquid interfaces, $n \geq 0.5$ is generally expected.[81] The values of n observed here easily exceeds this minimum requirement, indicating an adequate electrical contact between the electrode and the IL electrolyte. The spatial inhomogeneity of this interface, as reflected in the measured values of n, is comparable to that previously observed for a paper electrode of carbon nanotubes in $EtMeImEtSO_4$.[73]

4. Conclusions

We have synthesized novel mPEG-derivatized imidazolium iodides and studied the influence of chemical structure of the Im cation on the IL's density, viscosity, conductivity, and the temperatures of glass-transition, melting, and decomposition. Four different 1-alkyl-3-methylimidazolium iodide ILs were also synthesized and characterized, in order to understand how the ether oxygen atoms affect IL properties in comparison to ILs that do not contain these atoms. The PEGylated ILs showed satisfactory thermal stability, with decomposition temperatures higher than those of the C$_n$MeImI ILs. The mPEG16MeImI IL, with a longer mPEG tail, showed a higher melting temperature in DSC experiments. The PEG-derivatized ionic liquids showed glass transition temperatures in the range of −50 to −60 °C.

The viscosity, conductivity, and thermal-degradation temperature variations with chemical structure clearly indicate that the mPEG side chains of mPEG*n*ImI ILs interact with the Im cation and shield Coulombic interactions between Im and iodide anions. The weakened cation−anion interactions result in higher molar conductivities for mPEG*n*MeImI ILs than C$_n$MeImI ILs, in spite of their relatively high viscosities. In addition, the viscosities of mPEG*n*MeImI ILs were lower than that of HexMeImI (cf. Figure 3), and the molecular weight normalized viscosity was the lowest for mPEG16-MeImI and the highest for HexMeImI (see the Supporting Information). The reduction in viscosity compared to Hex-MeImI, however, occurs only when a relatively small alkyl group is attached to the second nitrogen atom of the Im ring, and not larger alkyl groups, such as *n*-butyl, that could interfere with the cation−tail interactions. The viscosities of mPEG*n*MeImI increased with an increase in the molecular weight of the IL, except at lower temperatures (close to room temperature) where this trend was reversed. The reversal of trends in the temperature dependencies of viscosity and ionic conductivity near room temperature is attributed to increased tail−tail interactions (nanoscale segregation) at lower temperatures, leading to aggregation of the mPEG*n*-MeImI molecules. Although the ring−tail hydrogen bonding interactions in ether-derivatized ILs with short ether tails, such as $-CH_2OCH_3$, $-CH_2CH_2OCH_3$, and $-CH_2CH_2O-CH_2CH_2OCH_3$, are expected to lower tail−tail segregation,[19] the ILs with the long mPEG16 and mPEG12 side chains showed side chain crystallization in DSC experiments.

Among the nine organic salts studied in this work, EtMeImI has the highest ionic conductivity in the liquid state. However, its solid state conductivity, at temperatures below about 50 °C, is about 2 orders of magnitude lower (cf. Figure 4c). The room-temperature conductivities of the mPEG*n*MeImI ionic liquids, on the other hand, are higher than that of EtMeImI. We attribute this effect to the lower viscosity and better solvation of the iodide anions in the PEGylated ILs.

The PEGylated IL, mPEG7MeImI, showed higher resistance against cathodic reduction compared to the C$_n$MeImI ILs, an effect that is associated with the protective sheath of the mPEG tail surrounding the cation. Moreover, the polarization resistance at the interface of the PEGylated IL and a glassy carbon electrode was relatively large, indicating a strongly nonfaradaic nature

of the interface. The electrical contact between the IL and the GC electrode was found to be satisfactory.

Because of their relatively high ionic conductivity, even without addition of salts such as LiI, the PEGylated imidazolium iodides are promising as electrolytes for electrochemical devices such as DSSCs. The charge carrier concentrations, and hence the ionic conductivities of the mPEG-derivatized ILs can be increased further by blending these ILs with iodide salts. The polar nature of the polyether side chains in the PEGylated ionic liquids permits dissolution of large amounts of these salts. The enhancement in the ionic conductivity of PEGylated imidazolium iodides using this approach will be discussed in a separate report.

Acknowledgment. Financial support from the Army Research Office Grant W911NF-05-1-0339 is gratefully acknowledged.

Supporting Information Available: DSC thermographs of mPEG7MeImI and EtMeImI, tables of viscosity and ionic conductivities of the mPEG-derivatized imidazolium ILs and the 1,3-dialkylimidazolium iodide ILs, VFT fit parameters for viscosity and conductivity data, viscosity and conductivity activation energies, EIS data for PrMeImI, cyclic voltammograms for $EtMeImEtSO_4$ and $EtMeImEtSO_4$ solution of LiI, and ^1H NMR spectra of mPEG12OTs, mPEG12I, mPEG12-MeImI, EtMeImI, PrMeImI, BuMeImI, HexMeImI, and $CDCl_3$ solvent (PDF). This material is available free of charge via the Internet at http://pubs.acs.org.

PEGylated Imidazolium Ionic Liquid Electrolytes: Thermophysical and Electrochemical Properties

Lalitha V. N. R. Ganapatibhotla,[1] Jianping Zheng,[2] Dipankar Roy,[2] Sitaraman Krishnan[1,]*

[1] Department of Chemical and Biomolecular Engineering, Clarkson University, Potsdam, NY 13699

[2] Department of Physics, Clarkson University, Potsdam, NY 13699

[*] To whom correspondence should be addressed. E-mail: skrishna@clarkson.edu.

Supporting Information

Differential Scanning Calorimetry. Figures S1a and S1b show the DSC thermograms of the mPEG7MeImI and EtMeImI ionic liquids (ILs), respectively.

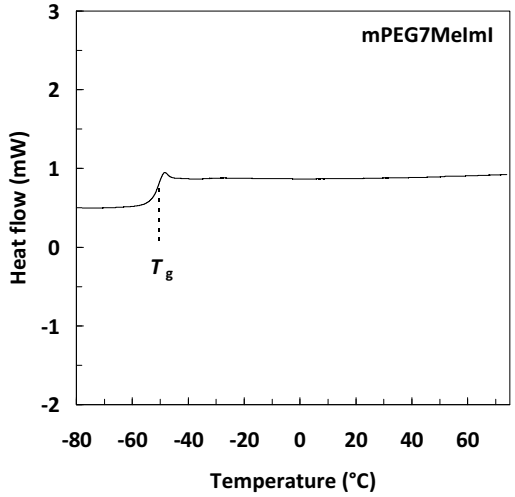

Figure S1. (a) DSC thermograms of mPEG7MeImI. The sample was scanned over a temperature range of 100 to −80 °C, and the thermogram obtained during the second heating cycle is shown.

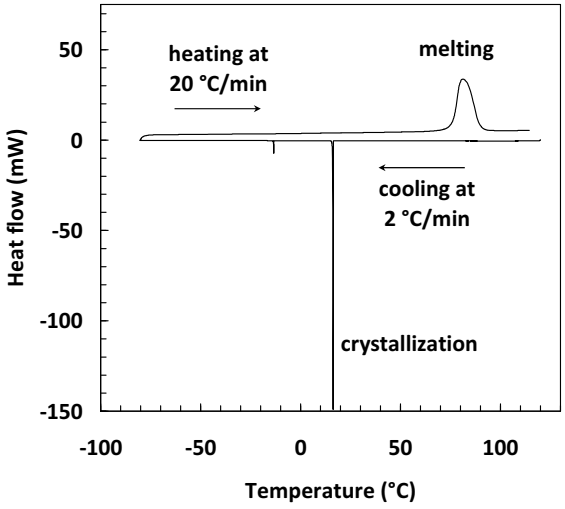

Figure S1. (b) DSC thermograms of EtMeImI acquired using a cooling rate of 2 °C/min and a heating rate of 20 °C/min. The sample was first heated to 120 °C and held at this temperature for 10 min. Data obtained during the first cooling and the second heating cycles are shown.

Viscosity. Table S1 gives the viscosities of the ILs synthesized in this work, at temperatures in the range of 20 to 95 °C. See Schemes 1 and 2 of the paper for chemical structures of these ILs. The viscosity data was fitted by the VFT equation, $\eta = \eta_0 \exp\{B/(T - T_0)\}$. The best-fit values of the parameters are reported in Table S2.

Table S1. Viscosity of mPEG*n*ImI and C$_n$MeImI ILs at different temperatures.

	Viscosity (cP)							
T (°C)	mPEG16 MeImI	mPEG12 MeImI	mPEG7 MeImI	mPEG7 BuImI	HexMeImI	BuMeImI	PrMeImI	EtMeImI
20	1327.4	1577.2	1717.9	2629.9	2633.0	1457.8	1062.0	n.d.
25	900.9	1025.7	1094.9	1675.0	1741.5	984.6	711.8	n.d.
30	626.0	698.5	720.6	1124.7	1175.0	672.7	489.3	n.d.
35	455.0	491.7	492.4	768.4	801.8	473.7	345.1	n.d.
40	333.2	353.7	347.7	535.2	563.5	340.1	250.6	n.d.
45	249.2	258.7	251.0	385.3	404.7	249.5	185.5	56.3
50	195.4	198.4	188.8	284.3	278.8	193.3	136.4	48.8
55	154.2	156.1	145.0	220.2	213.4	149.3	104.0	42.8
60	124.2	122.5	111.6	168.6	163.7	115.6	84.1	36.9
65	100.4	98.7	89.3	132.2	123.6	90.9	68.2	31.5
70	82.9	80.7	72.1	105.2	100.4	72.7	56.0	27.7
75	69.2	66.6	58.6	84.5	79.9	59.3	45.7	23.8
80	58.3	55.6	48.6	68.4	64.6	48.8	37.6	20.8
85	49.3	47.1	40.6	55.9	52.1	40.5	31.5	18.2
90	41.8	39.7	34.0	45.9	42.0	34.0	26.3	16.1
95	35.8	34.2	29.0	37.5	38.5	28.7	22.5	14.3

n.d. = not determined

Table S2. Parameters of the VFT equation, for temperature dependence of viscosity, in the temperature range of 20 to 95 °C.

	η_0 (cP)	B (K)	T_0 (K)	r^2
mPEG16MeImI	0.216	933.09	186.15	0.9999
mPEG12MeImI	0.228	870.55	194.68	1.0000
mPEG7MeImI	0.150	907.30	196.12	1.0000
mPEG7BuImI	0.0505	1283.32	174.90	0.9999
HexMeImI	0.0349	1358.99	172.52	0.9996
BuMeImI	0.0435	1291.30	169.26	1.0000
PrMeImI	0.0811	1039.82	183.58	0.9998

Table S3 gives the viscosity activation energy values for the ILs, calculated using the Arrhenius equation.

Table S3. Activation energy for viscous flow, in the temperature ranges of 20–55 and 60–95 °C.

	E_a (kJ/mol)	
	60–95 °C	20–55 °C
mPEG16MeImI	36.02	49.22
mPEG12MeImI	37.15	52.91
mPEG7MeImI	39.30	56.52
mPEG7BuImI	43.54	56.89
HexMeImI	43.07	57.77
BuMeImI	40.45	52.29
PrMeImI	38.68	52.95
EtMeImI	27.78	n.d.

It is seen from the data shown in Table S1 that, within each set of ILs, the viscosity increases with an increase in the side chain length and, therefore, the molecular weight of the IL. The effect of molecular weight on viscosity is evident from the plot of the Orrick and Erbar normalized viscosity, $\eta/\rho_L M$, where η (cP) is the liquid viscosity at temperature, T (K), ρ_L (g/cm^3) is the liquid density at room temperature, and M (g/mol) is the molar mass of the IL.[1] Figure S2 shows that side chain ether groups indeed play a significant role in lowering the viscosity of the imidazolium salts.

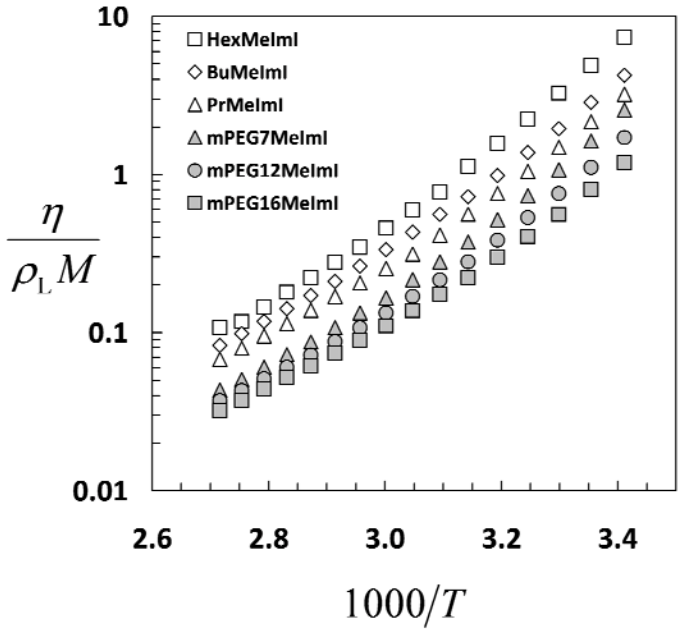

Figure S2. Molar mass and density normalized viscosity vs temperature for alkyl- and mPEG-derivatized ILs.

Ionic Conductivity. Figure S3 shows illustrative EIS results, in the form of Nyquist plots, used here to determine the conductivities of the ILs. Z' and Z'' are the real and imaginary components, respectively, of the complex impedance, Z, of the test cell. The EEC model in the inset is obtained by CNLS fitting these data to the calculated impedance spectra of the model circuit. The constant phase element (CPE), Q, in the EEC represents the frequency dispersed net capacitance of the two electrode-electrolyte interfaces of the experimental cell,[2] and is only necessary to accurately fit the full frequency range of the

calculated and experimental impedance spectra. Information about IL conductivity is derived from the CNLS-calculated bulk electrolyte resistance, R_s, which in combination with the pre-determined cell constant, L/A, provides the specific conductivity, λ, of the IL as a function of temperature.

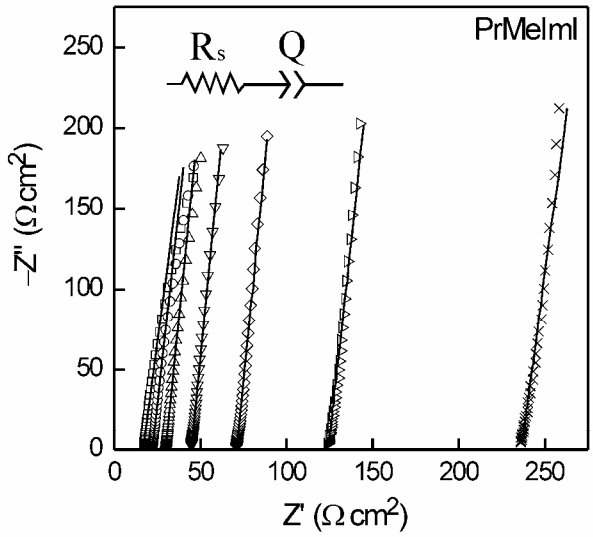

Figure S3. Nyquist plots of the real (Z') and imaginary (Z'') parts of the complex impedance of PrMeImI in a two-electrode test cell. The symbols represent experimental data at different temperatures and the lines are complex nonlinear least-square fits to the data using the circuit model shown in the inset; T = 90 °C (□), 80 °C (○), 70 °C (△), 60 °C (▽), 50 °C (◇), 40 °C (▷), and 30 °C (×).

Table S4 gives the conductivities of the ILs, at different temperatures, in the range of 10 to 105 °C. The ionic conductivity data could be fitted well by the VFT equation, $\lambda = \lambda_0 \exp\left\{-C/\left(T - T_0^{'}\right)\right\}$. The best-fit values of the parameters are listed in Table S5.

Table S4. Conductivity of mPEG*n*ImI and C_nMeImI ILs at different temperatures.

	Conductivity (mS/cm)							
T (°C)	mPEG16 MeImI	mPEG12 MeImI	mPEG7 MeImI	mPEG7 BuImI	HexMeImI	BuMeImI	PrMeImI	EtMeImI
10	0.035	0.029	0.029	0.019	0.066	0.101	0.188	0.033
15	0.055	0.052	0.051	0.033	0.105	0.160	0.299	0.046
20	0.084	0.080	0.082	0.050	0.160	0.241	0.456	0.061
25	0.112	0.119	0.128	0.068	0.239	0.371	0.682	0.079
30	0.158	0.172	0.194	0.109	0.357	0.550	0.994	0.104
35	0.215	0.241	0.282	0.154	0.512	0.791	1.398	0.138
40	0.288	0.327	0.390	0.212	0.712	1.094	1.890	0.194
45	0.379	0.438	0.523	0.285	0.968	1.474	2.524	0.282
50	0.483	0.565	0.696	0.380	1.299	1.960	3.327	0.390
55	0.611	0.717	0.896	0.492	1.705	2.557	4.261	8.976
60	0.753	0.891	1.129	0.627	2.159	3.244	5.270	10.660
65	0.915	1.101	1.396	0.786	2.687	4.028	6.522	12.276
70	1.099	1.335	1.719	0.979	3.239	4.957	7.899	14.507
75	1.304	1.598	2.004	1.200	3.970	5.796	9.067	16.443
80	1.524	1.879	2.317	1.435	4.755	6.812	10.613	18.841
85	1.747	2.152	2.671	1.672	5.724	7.995	12.315	21.218
90	2.003	2.458	3.069	2.000	6.765	9.309	14.003	24.379
95	2.268	2.701	3.468	2.311	7.934	10.481	15.570	26.993
100	2.512	2.961	3.883	2.629	9.070	11.476	17.247	30.462
105	n.d.	n.d	4.267	n.d.	10.350	12.460	18.909	33.907
110	n.d.	n.d.	n.d.	n.d.	n.d.	13.234	20.677	37.684

n.d. = not determined

Table S5. Parameters of the VFT equation, for temperature dependence of ionic conductivity, in the temperature range of 20 to 95 °C.

	λ_0 (mS/cm)	C (K)	$T_0^{'}$ (K)	r^2
mPEG16MeImI	249.49	844.45	188.03	0.9997
mPEG12MeImI	172.92	671.08	205.81	0.9997
mPEG7MeImI	183.82	612.05	213.52	0.9997
mPEG7BuImI	738.00	1076.14	181.17	0.9997
BuMeImI	837.88	724.07	203.68	0.9989
PrMeImI	872.28	648.33	206.94	0.9994
EtMeImI	4742.76	1158.59	143.79	0.9999

Table S6 gives the conductivity activation energy values for the ILs, calculated using the Arrhenius equation.

Table S6. Arrhenius parameters, for temperature dependence of ionic conductivity, in the temperature range of 60 to 95°C.[a]

	$\ln(\lambda_0$ / mScm$^{-1})$	$E_a^{'}$(kJ/mol)	r^2
mPEG16MeImI	11.322	32.07	0.9974
mPEG12MeImI	11.685	32.56	0.9927
mPEG7MeImI	11.819	32.28	0.9950
mPEG7BuImI	13.250	37.91	0.9977
HexMeImI	14.481	37.95	0.9997
BuMeImI	13.503	34.04	0.9970
PrMeImI	13.034	31.38	0.9952
EtMeImI	12.290	27.50	0.9993

[a] $\lambda = \lambda_0 \exp\left(-E_a^{'}/RT\right)$; r is the Pearson product-moment correlation coefficient for the linear fit of $\ln\lambda$ vs $1/T$.

Cyclic Voltammetry of mPEG7MeImI. To confirm that the current features observed within the electrochemical window of mPEG7MeImI, showing peak-like signature behavior of redox reactions, are associated with the I^-/I_3^- species, additional CV experiments were performed by adding 2.5 mM LiI (iodide concentration close to that in mPEG7MImI) to an iodide-free IL, 1-ethyl-3-methyl imidazolium ethylsulfate ($EtMeImEtSO_4$), and keeping the potential scale the same as that used in CV of mPEG7MeImI (cf. Figure S4a).

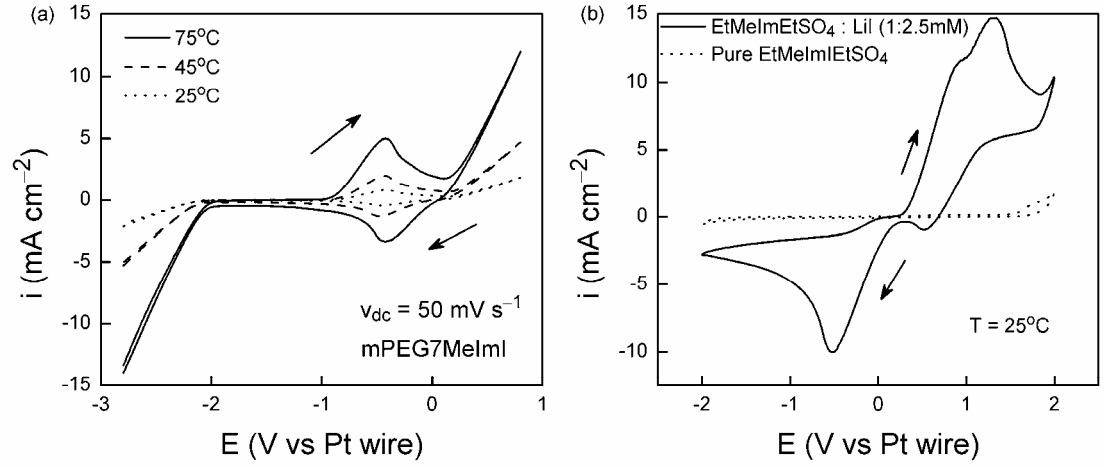

Figure S4. Cyclic voltammograms of: (a) mPEG7MeImI at different temperatures, and (b) the IL $EtMeImSO_4$ and a solution of LiI in $EtMeImEtSO_4$ at 25 °C.

The results of these experiments are shown in Figure S4b, where a clear oxidation feature is observed in the positive voltage scan. The dashed line plot in the same panel was recorded with LiI free $EtMeImEtSO_4$, where no redox features of faradaic reactions were observed. Based on previously published results,[3] the anodic current features of the solid line plot in Figure S4 can be associated with the two-step oxidation of iodide to I_2: $3I^- \rightarrow I_3^- + 2e^-$, followed by $2I_3^- \rightarrow 3I_2 + 2e^-$, with a net reaction of the form, $2I^- \rightarrow I_2 + 2e^-$. The occurrence of this reaction was also detected visually, as the electrolyte turned brown during the positive CV scan around 0.2 V, indicating the generation of I_2 at this potential. The features of the two oxidation steps were partially resolved in the LiI containing electrolyte.

The reverse voltage scan in Figure S4b shows the current peaks associated with the reduction of I_2 (reverse steps of the aforementioned oxidation reactions). However, due to mass transfer limitation, this

reaction was controlled mostly by interfacial species (rather than by the I_2 from the bulk solution), and some of the dissolved I_2 remained unreduced during the CV scan. This caused the electrolyte to retain its brown color acquired during the positive scan. The reduction peak observed in Figure S4b falls essentially in the same voltage region where the corresponding cathodic peak is observed in Figure S4a. The I^- oxidation peaks in the two panels are noticeably displaced with respect to each other because, the relative strengths and the surface densities of I^- and the IL anion, $EtSO_4^-$, on GC are likely to be different from the corresponding case for mPEG7MIm. Nevertheless, the overall similarities between the redox current peaks observed in the two panels of Figure S4 support the inference that these intermediate peaks in mPEG7MeImI are due to redox reactions of $I^-/I_3^-/I_2$.

^{1}H NMR Spectroscopy. The NMR spectra of of the tosylate ester of mPEG12 are shown in Figures S5a and S5b. The ^{1}H NMR spectra of mPEG12 iodide are shown in Figures S6a and S6b. Figures S7a–c are the ^{1}H-NMR spectra of the mPEG12MeImI IL. The NMR spectra of 1-ethyl-3-methylimidazolium iodide (EtMeImI), 1-*n*-propyl-3-methylimidazolium iodide (PrMeImI), 1-*n*-butyl-3-methylimidazolium iodide (BuMeImI), and 1-*n*-hexyl-3-methylimidazolium iodide (HexMeImI), are shown in Figures S8, S9, S10, and S11, respectively. Figure S12 is the ^{1}H-NMR spectrum of the deuterated NMR solvent, $CDCl_3$. The peak due to residual $CHCl_3$ is seen at 7.6 ppm, while the singlet peak due to HOH (the moisture in the solvent) is observed at 1.54 ppm, as expected.[4] In the NMR spectra of the ILs, the HOH singlet appears at about 1.8 ppm for mPEG12MeImI (cf. Figure S7c), EtMeImI (cf. Figure S8b), and PrMeImI (cf. Figure S9a), at about 1.71 ppm for BuMeImI (cf. Figure S10b), and at about 1.68 ppm for HexMeImI (cf. Figure S11b).

The moisture concentration in the IL can be estimated by subtracting the contribution of the solvent moisture to the area of the HOH singlet in the ^{1}H NMR spectrum of the IL. The concentration of water in the IL is then given by:

$$\text{wt \% HOH} = \frac{3M_{\text{HOH}}\left(A_{\text{HOH}} - \alpha A_{\text{CHCl}_3}\right)}{3M_{\text{HOH}}\left(A_{\text{HOH}} - \alpha A_{\text{CHCl}_3}\right) + 2M_{\text{IL}}A_{\text{NCH}_3}} \times 100$$

where M_{HOH} and M_{IL} are the molecular weights of water and IL, respectively; A_{HOH} and A_{CHCl_3} are the areas under the water singlet and $CHCl_3$ singlet in the NMR spectrum of the IL; and A_{NCH_3} is the area under the singlet (at about 4.1 ppm) due to protons of the methyl group that is attached to the imidazolium ring. The variable α is the ratio of the areas of the HOH peak (at 1.54 ppm) and $CHCl_3$ peak (at 7.26 ppm) in the spectrum of the $CDCl_3$ solvent handled and analyzed under the same conditions as those of the test solution. Ideally, $\alpha = 0$, but trace water is inevitable in NMR solvents because of the manufacturing process and solvent storage conditions.[5] Therefore, α is usually greater than 0, and is expected to increase as the solvent ages and absorbs moisture. The water content determined using this procedure is only an estimate because our calculations ignore water in the form of HOD or DOD, which could be formed by deuterium exchange. Nevertheless, we used this method for estimating the moisture content because the accuracy of the conventional coulometric Karl Fischer titration (that relies on the determination of charge required to generate I_2 from I^- ions) is questionable in the case of iodide containing ILs.

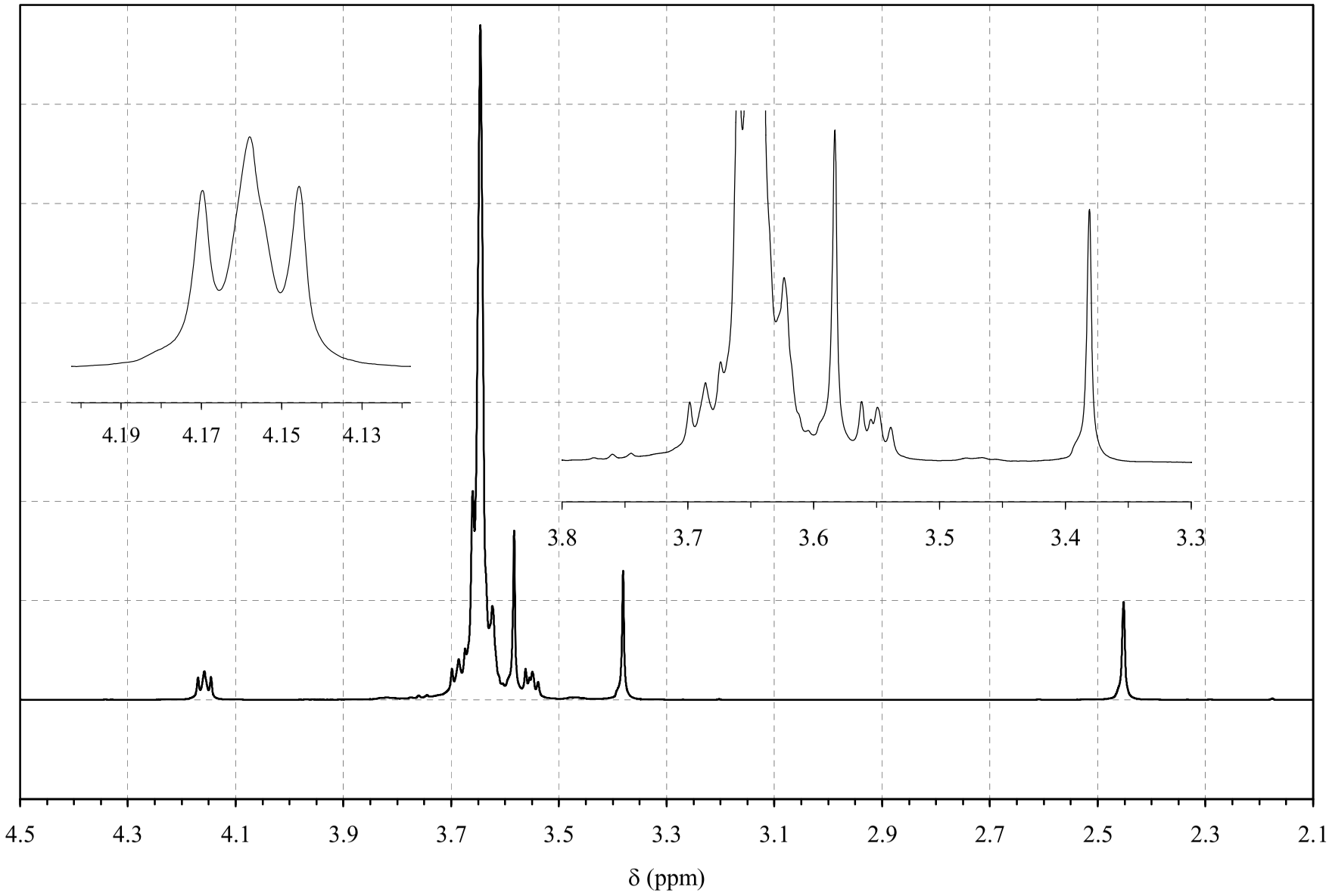

Figure S5. (a) ^{1}H NMR spectrum of mPEG12 tosylate, $CH_3O(CH_2CH_2O)_{11}CH_2CH_2OTs$. The crude product also contained $CH_3O(CH_2CH_2O)_{11}CH_2CH_2OH$.

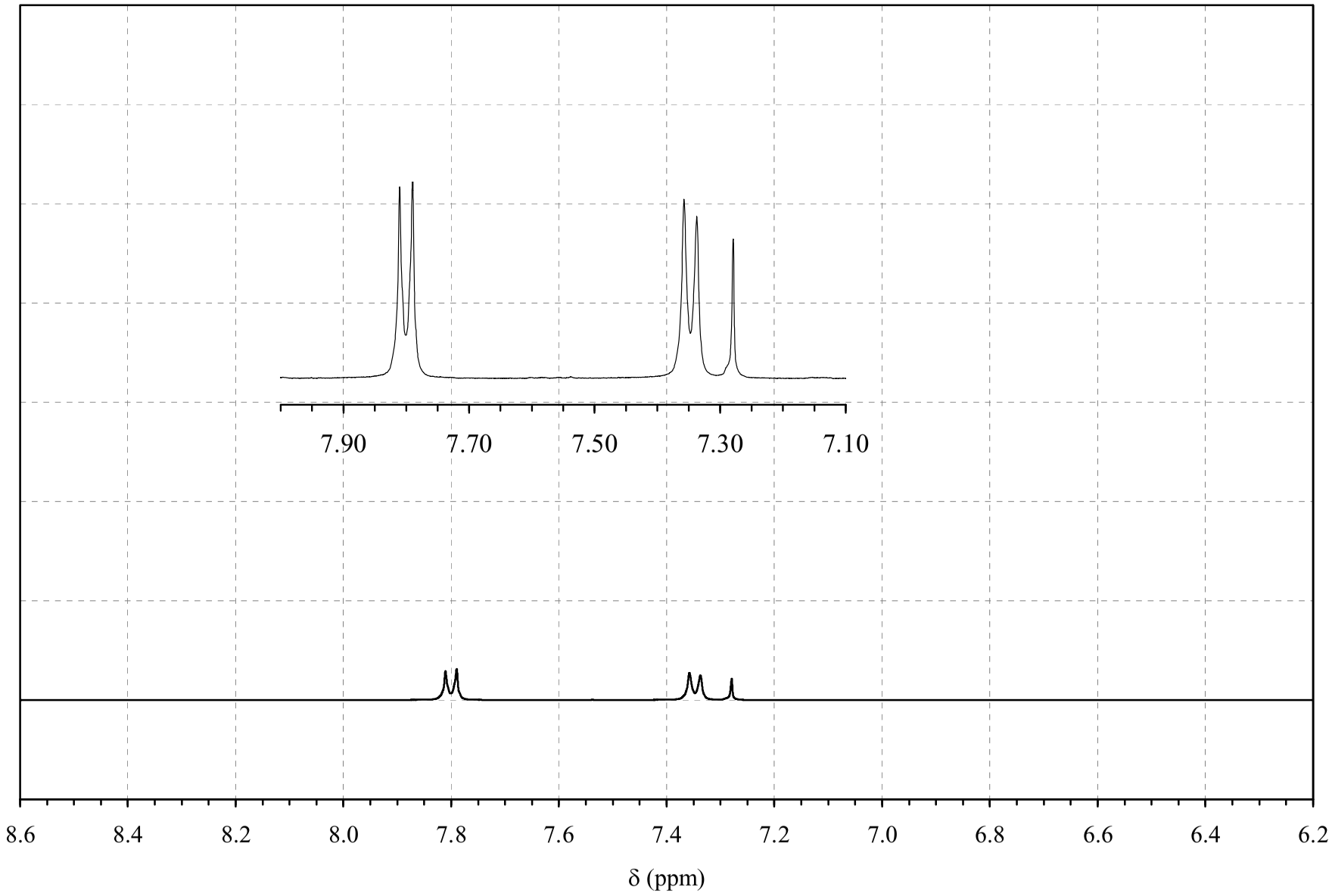

Figure S5. (b) ^{1}H NMR spectrum of mPEG12 tosylate, $CH_3O(CH_2CH_2O)_{11}CH_2CH_2OTs$. The crude product also contained $CH_3O(CH_2CH_2O)_{11}CH_2CH_2OH$.

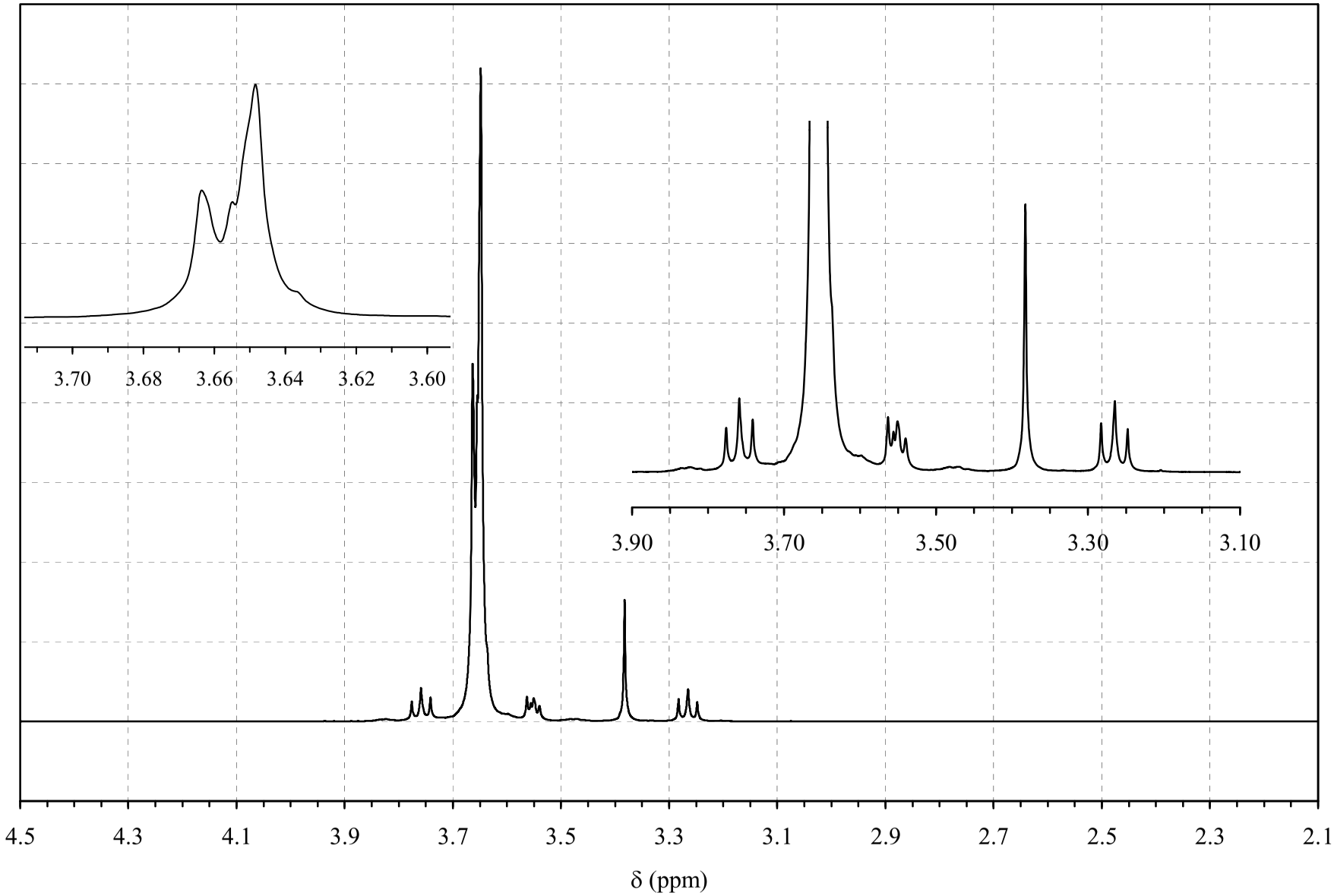

Figure S6. (a) ^{1}H NMR spectrum of mPEG12 iodide, $CH_3O(CH_2CH_2O)_{11}CH_2CH_2I$. The crude product also contained $CH_3O(CH_2CH_2O)_{11}CH_2CH_2OH$.

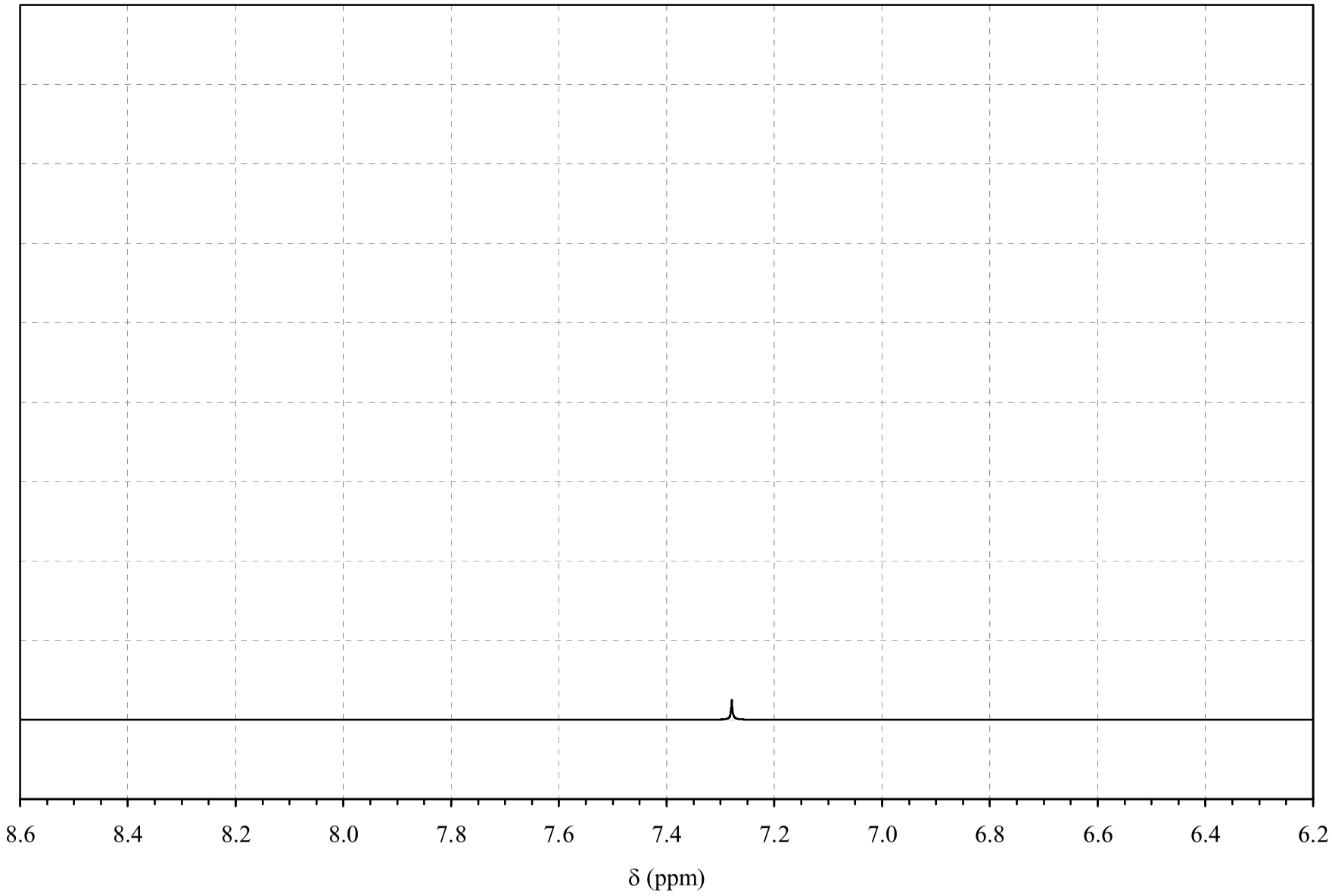

Figure S6. (b) ^{1}H NMR spectrum of mPEG12 iodide, $CH_3O(CH_2CH_2O)_{11}CH_2CH_2I$. The spectrum shows complete disappearance of the peaks due to aryl ring protons (at 7.80 and 7.35 ppm) that are present in the mPEG12 tosylate precursor.

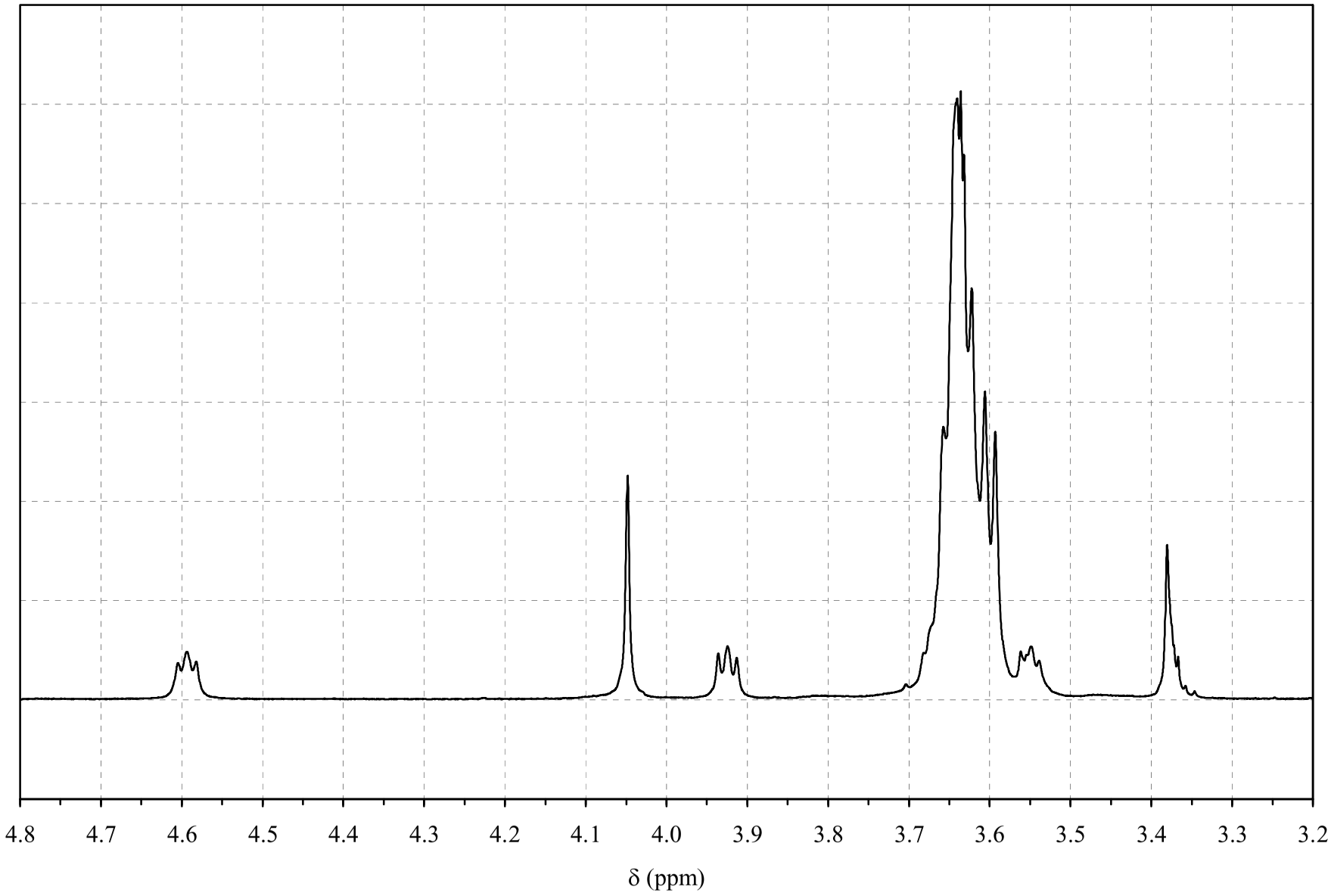

Figure S7. (a) ^{1}H NMR spectrum of mPEG12MeImI.

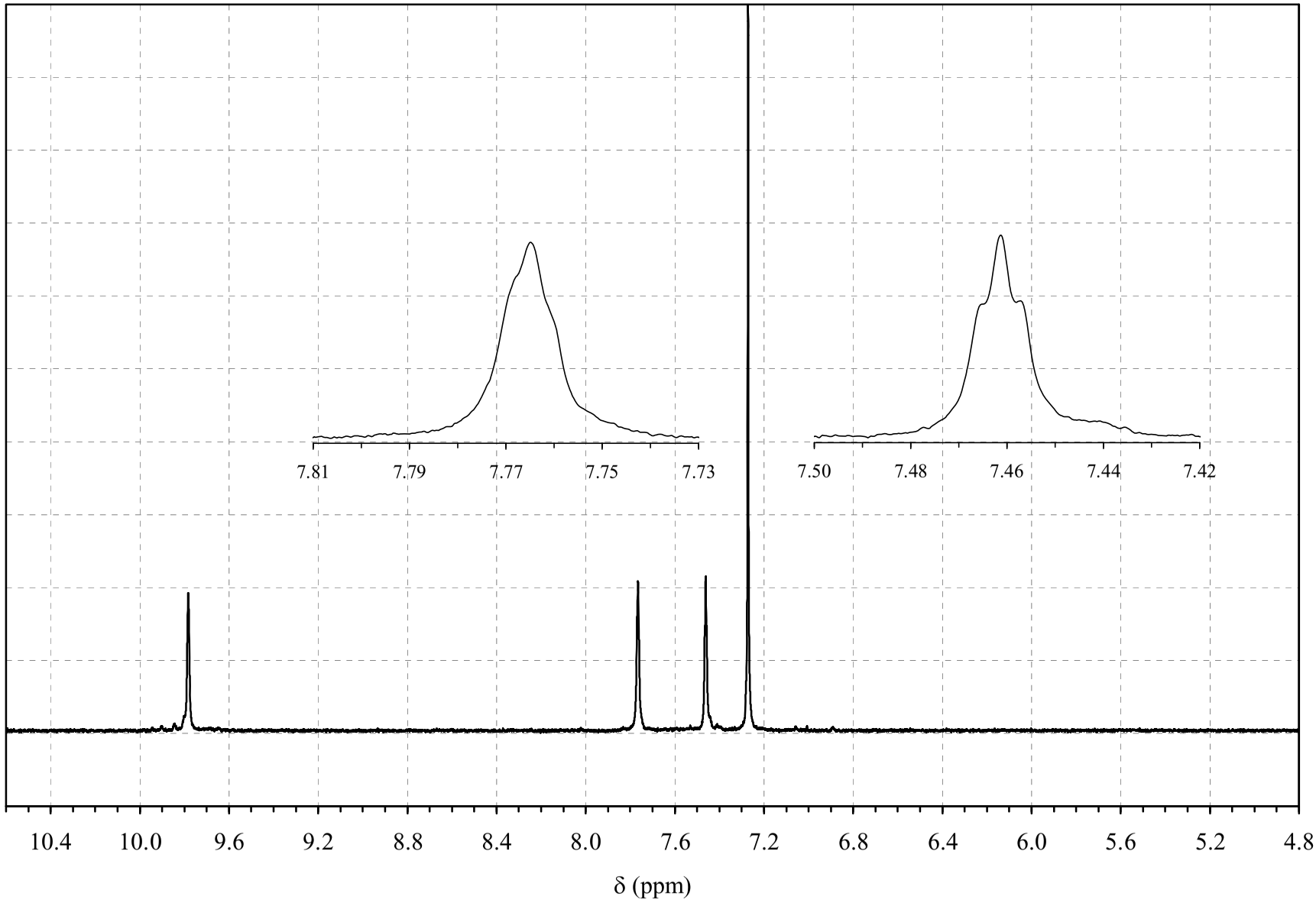

Figure S7. (b) ^{1}H NMR spectrum of mPEG12MeImI.

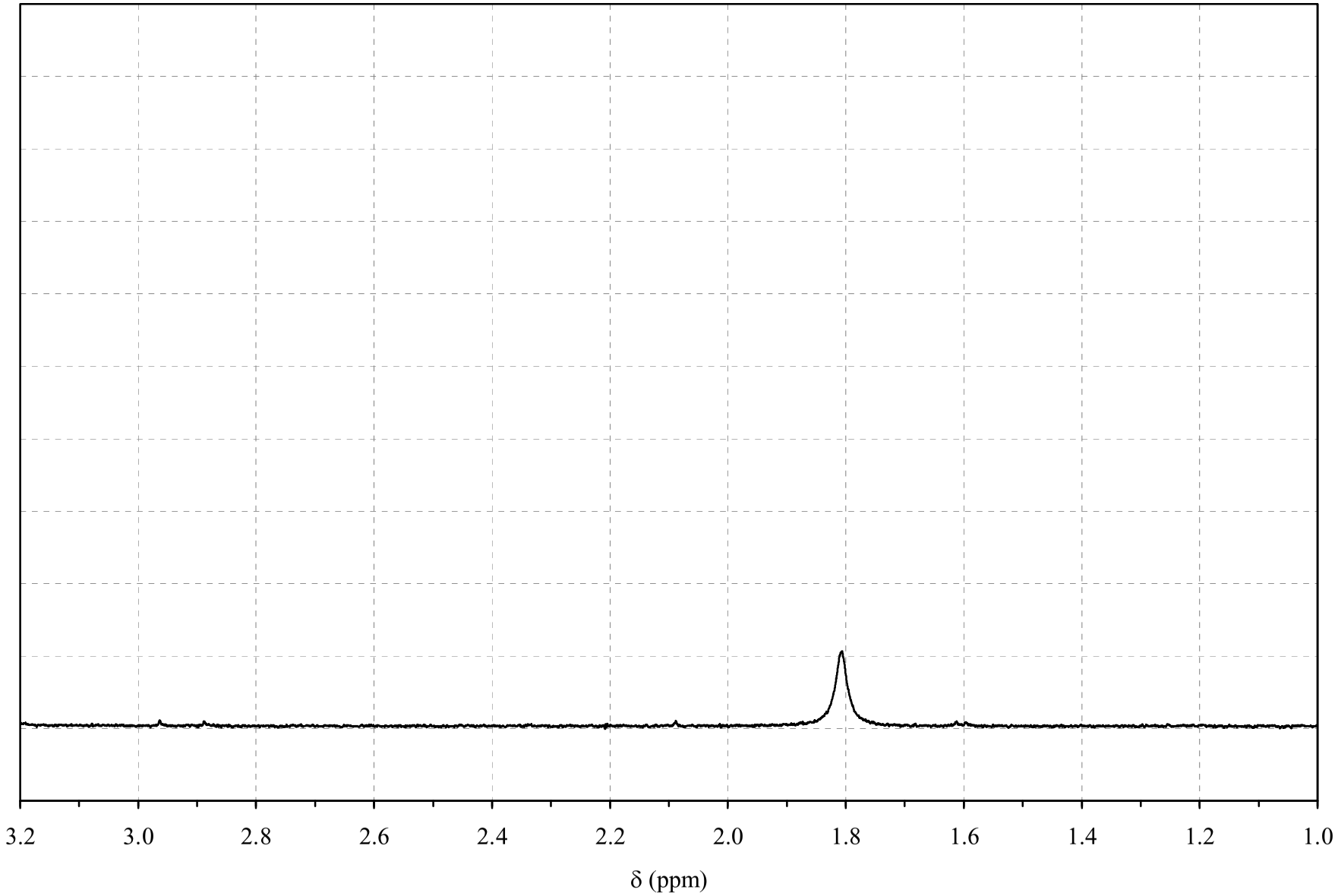

Figure S7. (c) ^{1}H NMR spectrum of mPEG12MeImI.

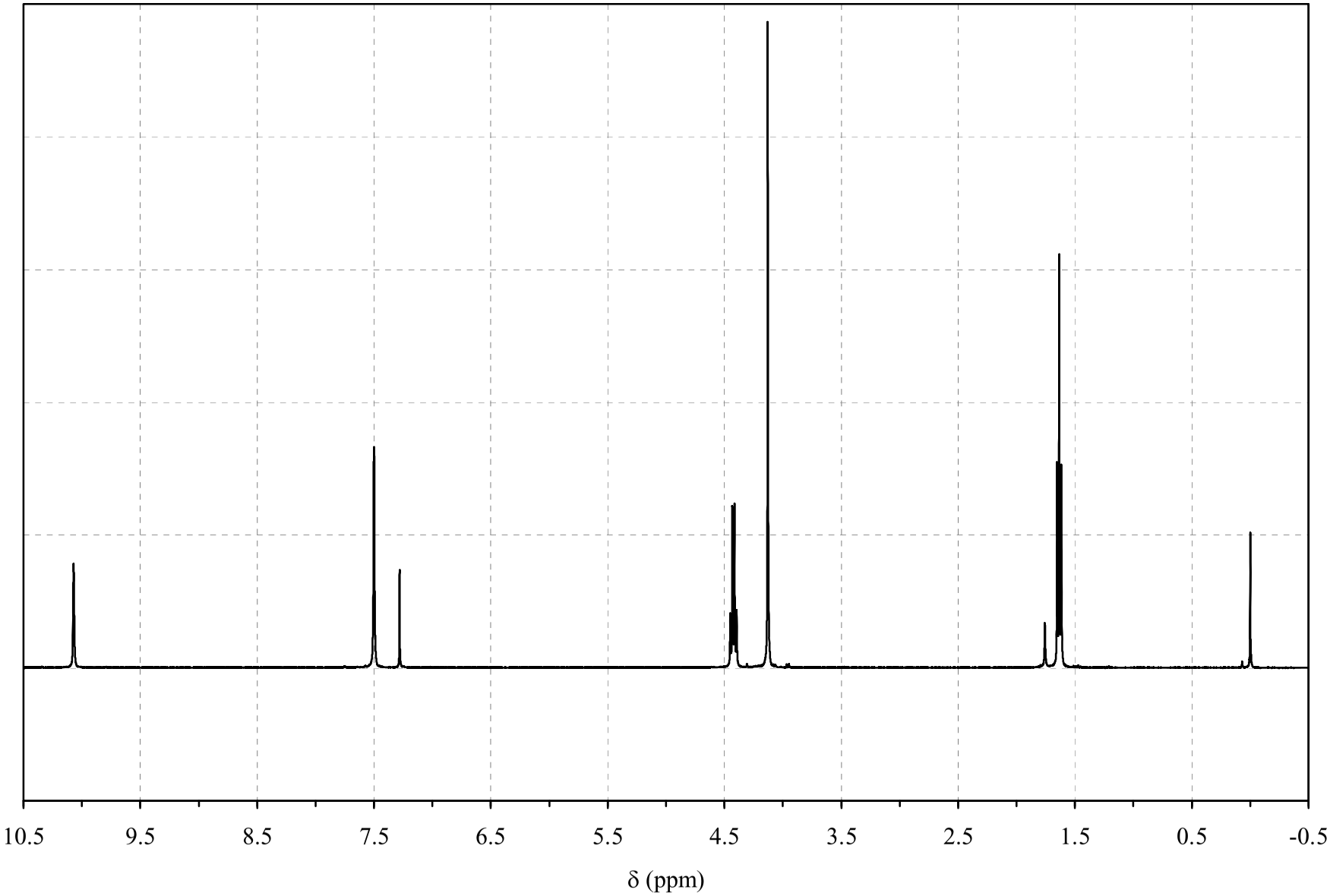

Figure S8. (a) ^{1}H NMR spectrum of 1-ethyl-3-methylimidazolium iodide (EtMeImI).

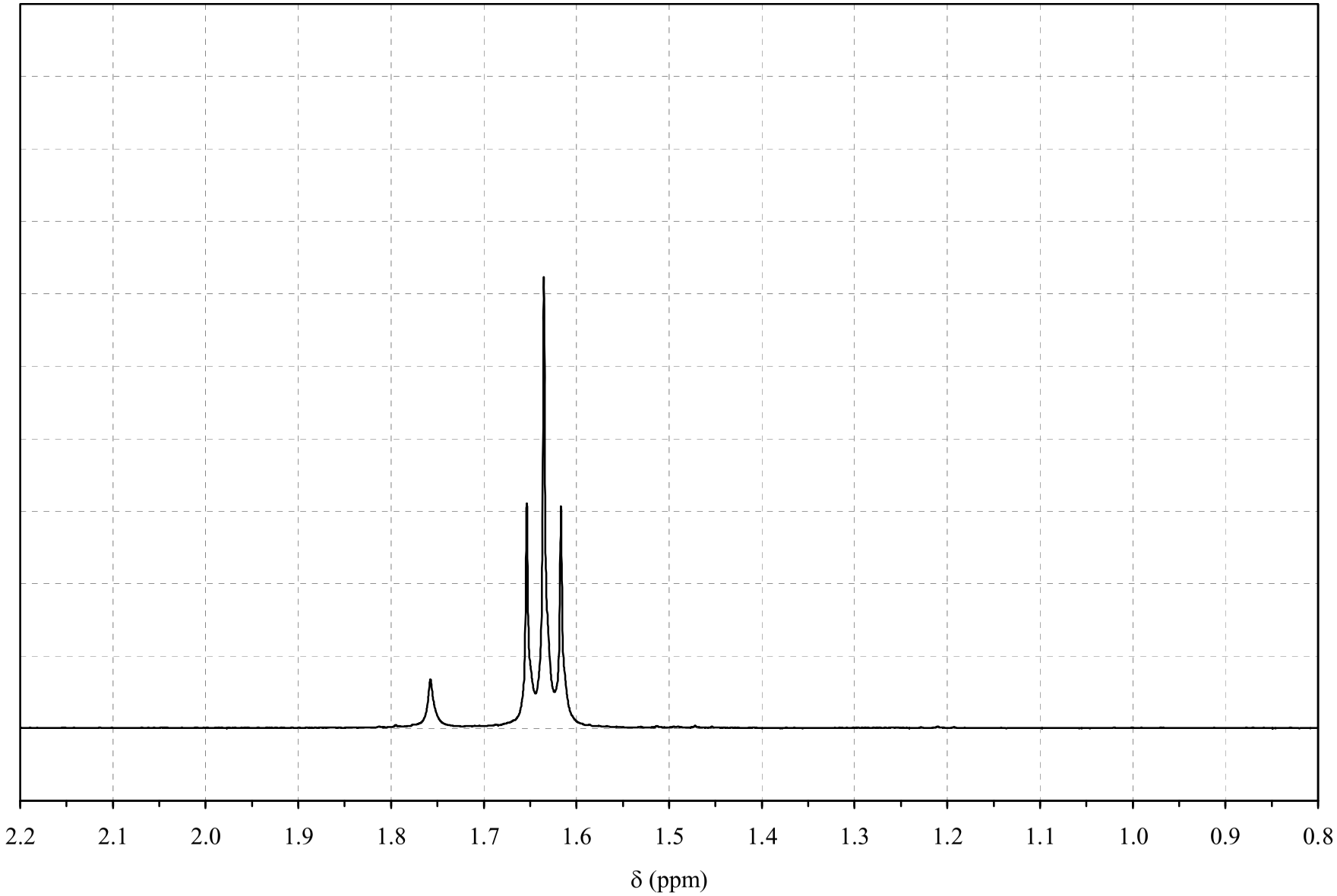

Figure S8. (b) ^{1}H NMR spectrum of 1-ethyl-3-methylimidazolium iodide (EtMeImI).

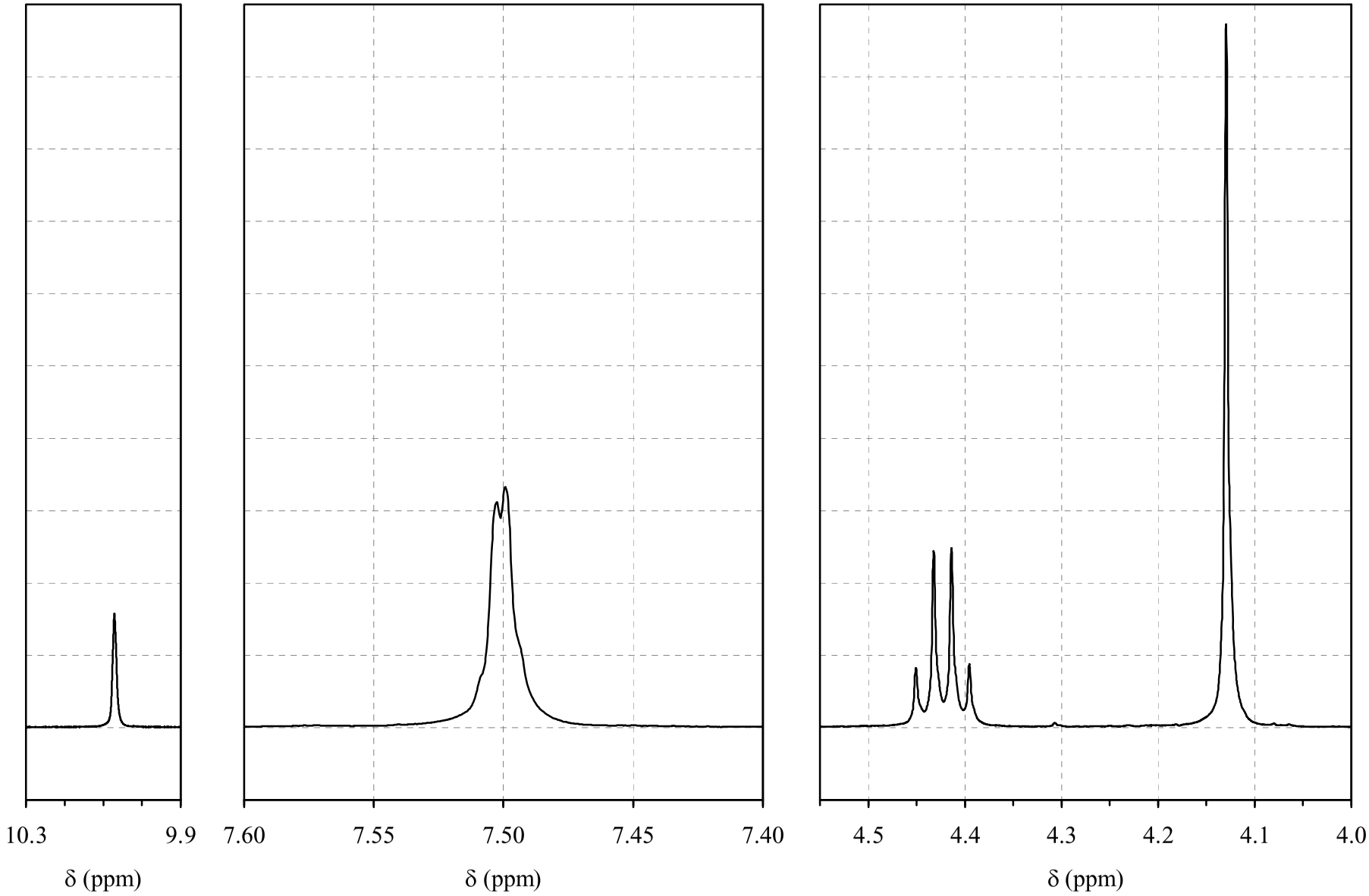

Figure S8. (c) ^{1}H NMR spectrum of 1-ethyl-3-methylimidazolium iodide (EtMeImI).

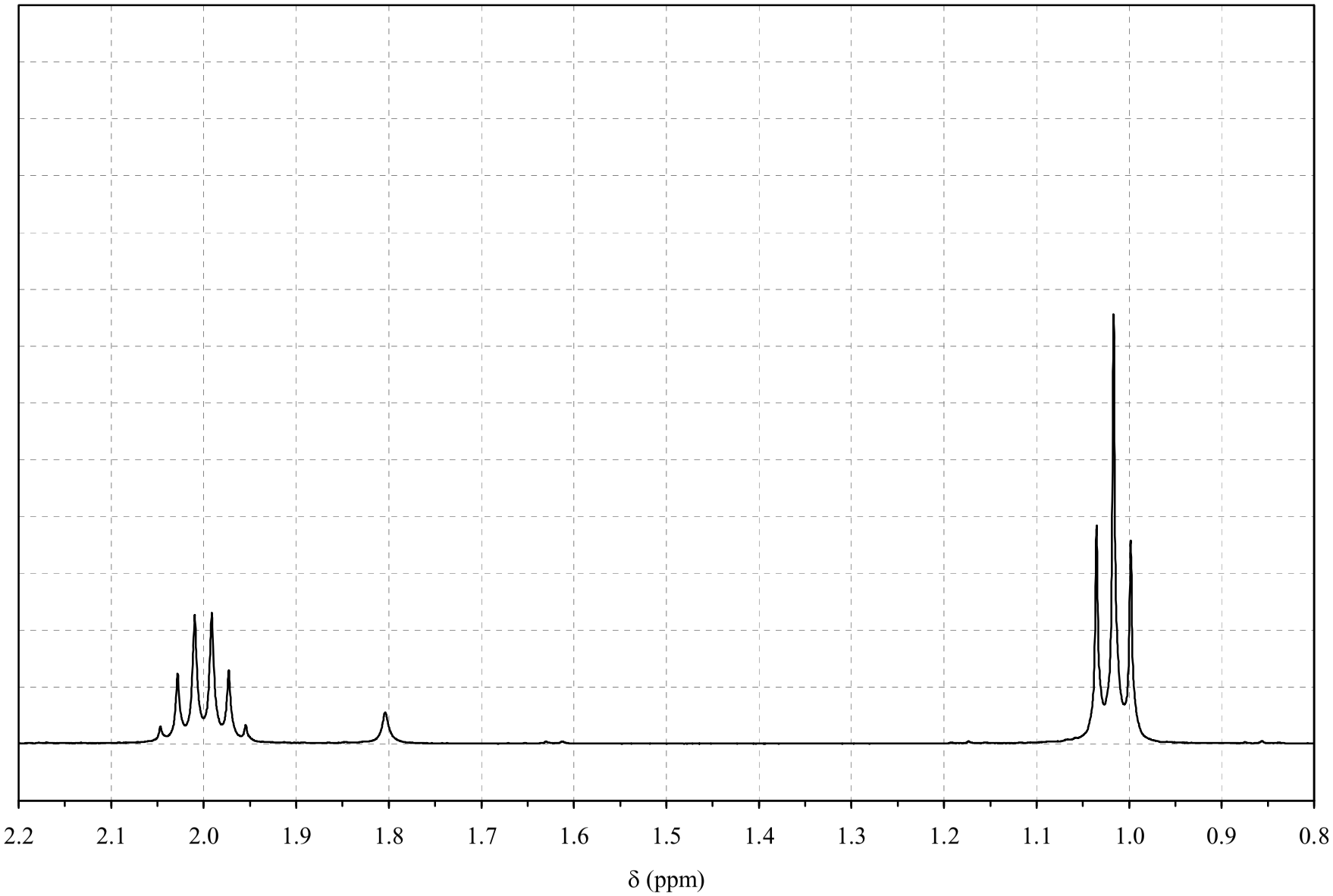

Figure S9. (a) ^{1}H NMR spectrum of 1-*n*-propyl-3-methylimidazolium iodide (PrMeImI).

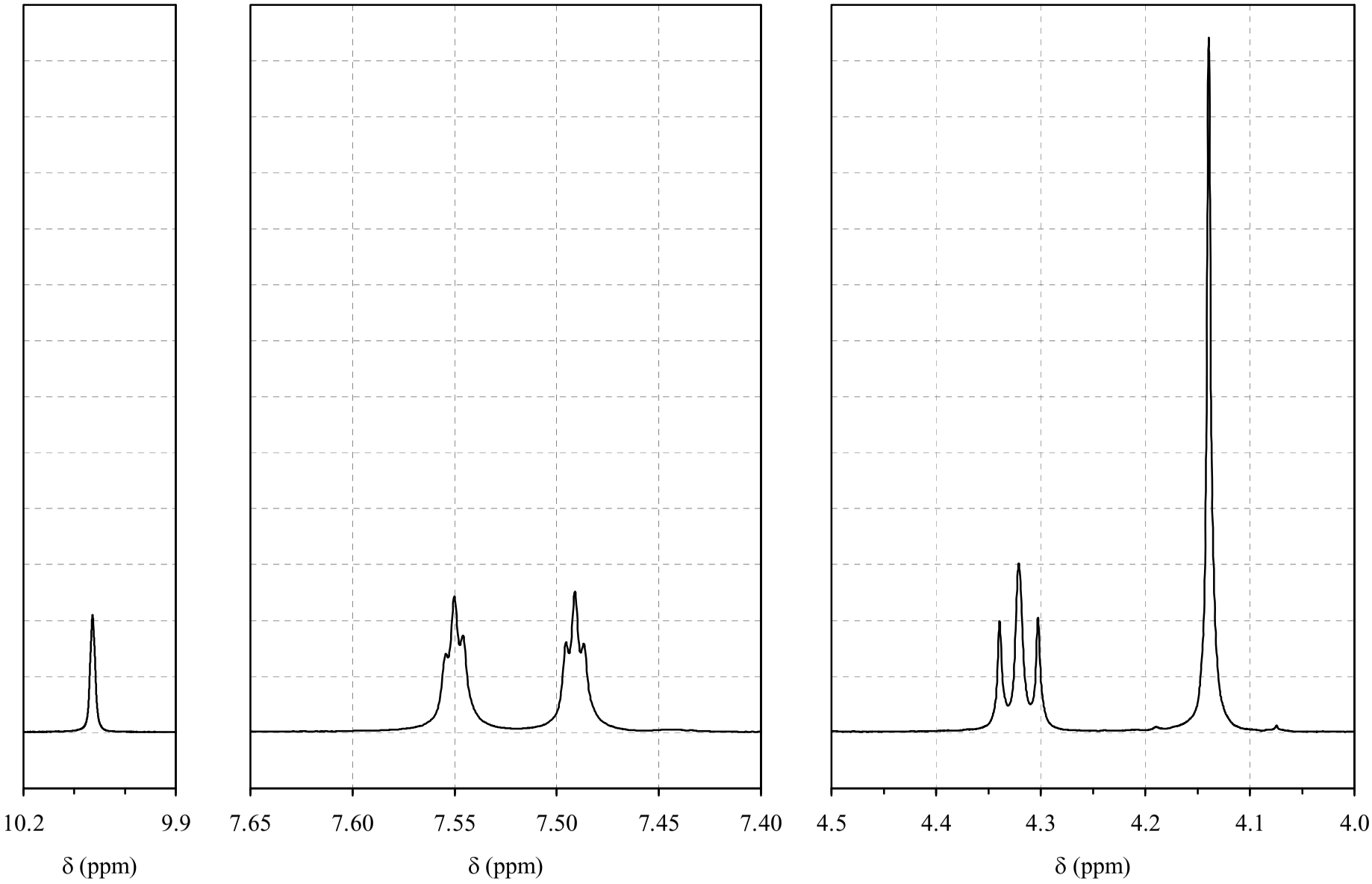

Figure S9. (b) ^{1}H NMR spectrum of 1-*n*-propyl-3-methylimidazolium iodide (PrMeImI).

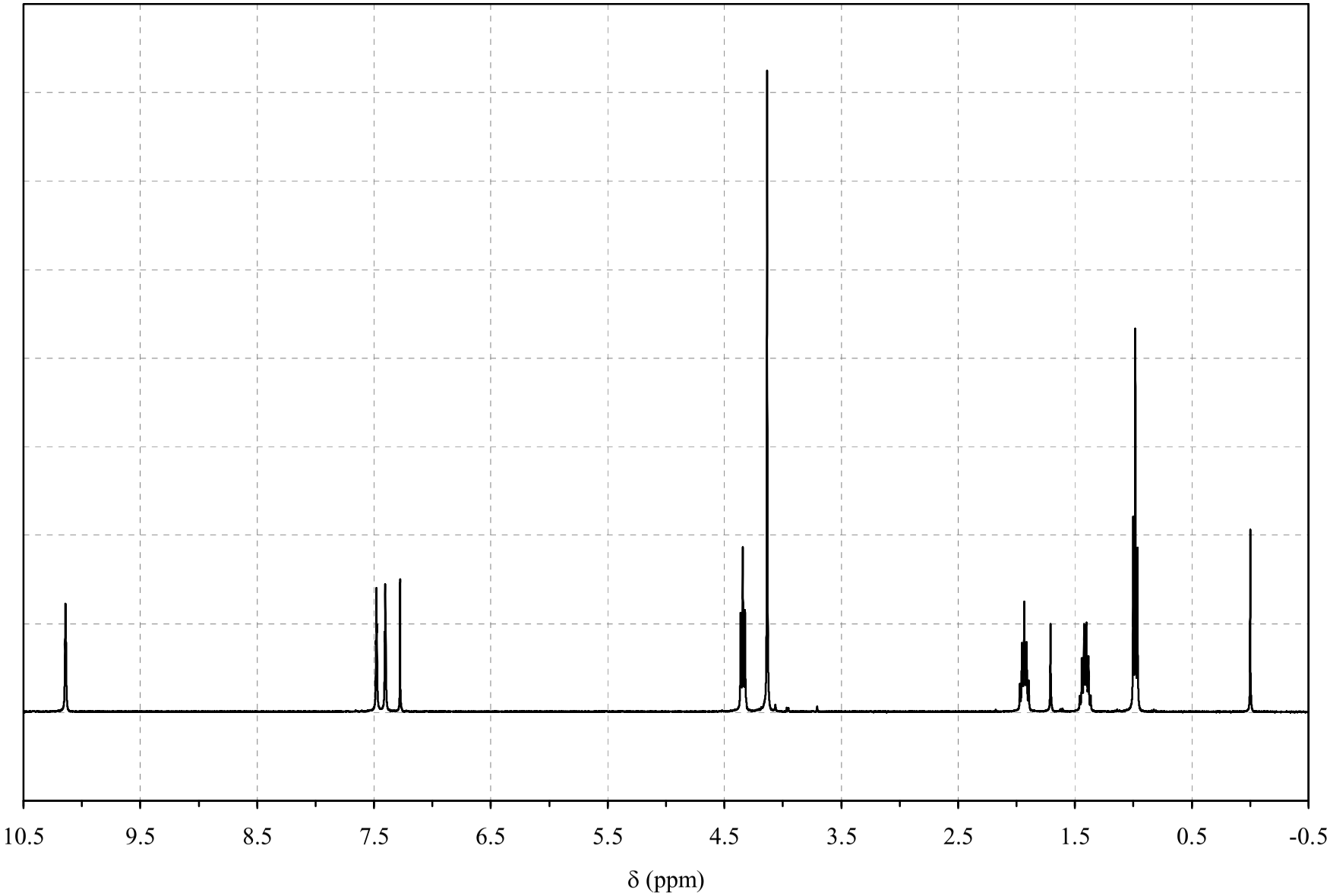

Figure S10. (a) ^{1}H NMR spectrum of 1-*n*-butyl-3-methylimidazolium iodide (BuMeImI).

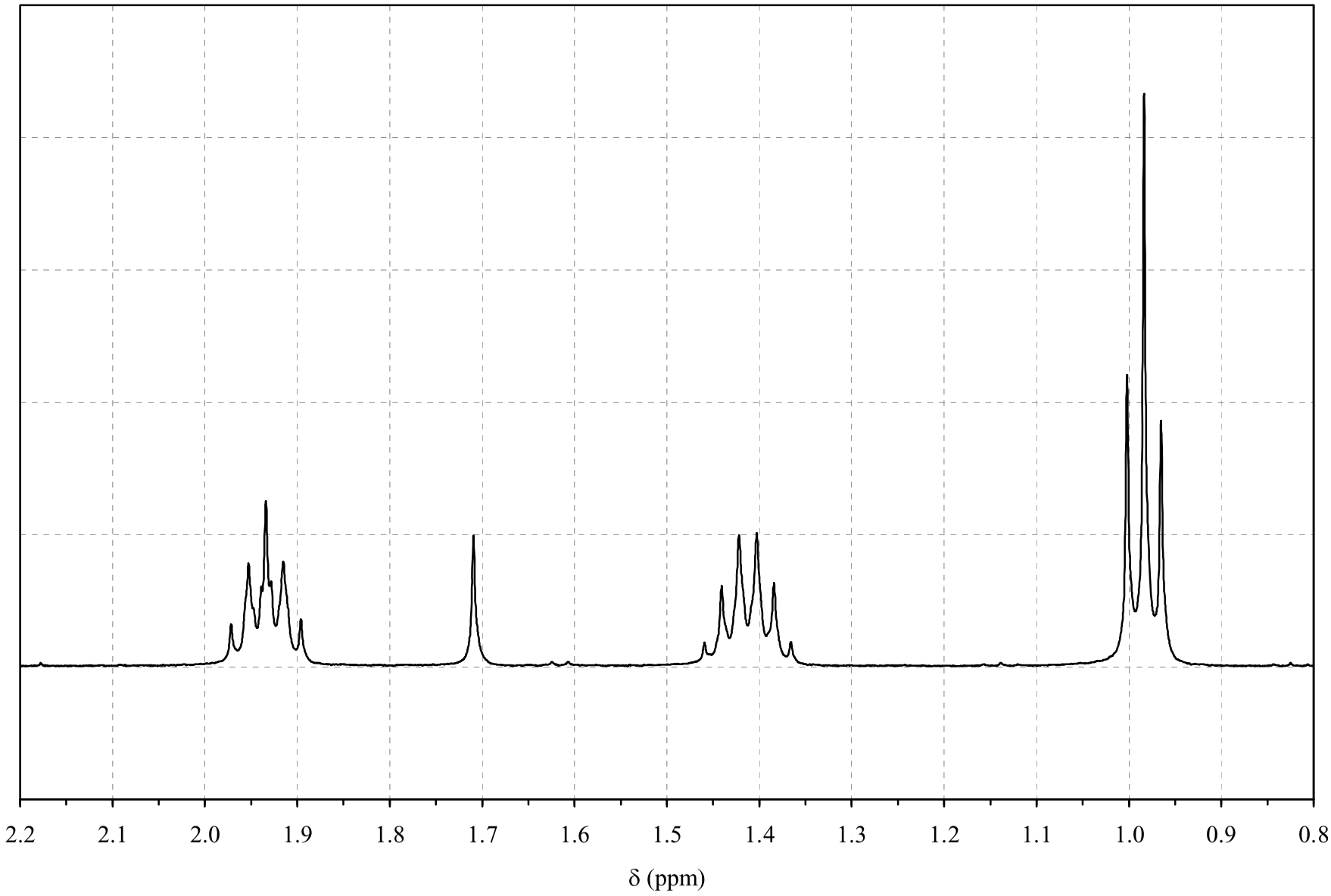

Figure S10. (b) ^{1}H NMR spectrum of 1-*n*-butyl-3-methylimidazolium iodide (BuMeImI).

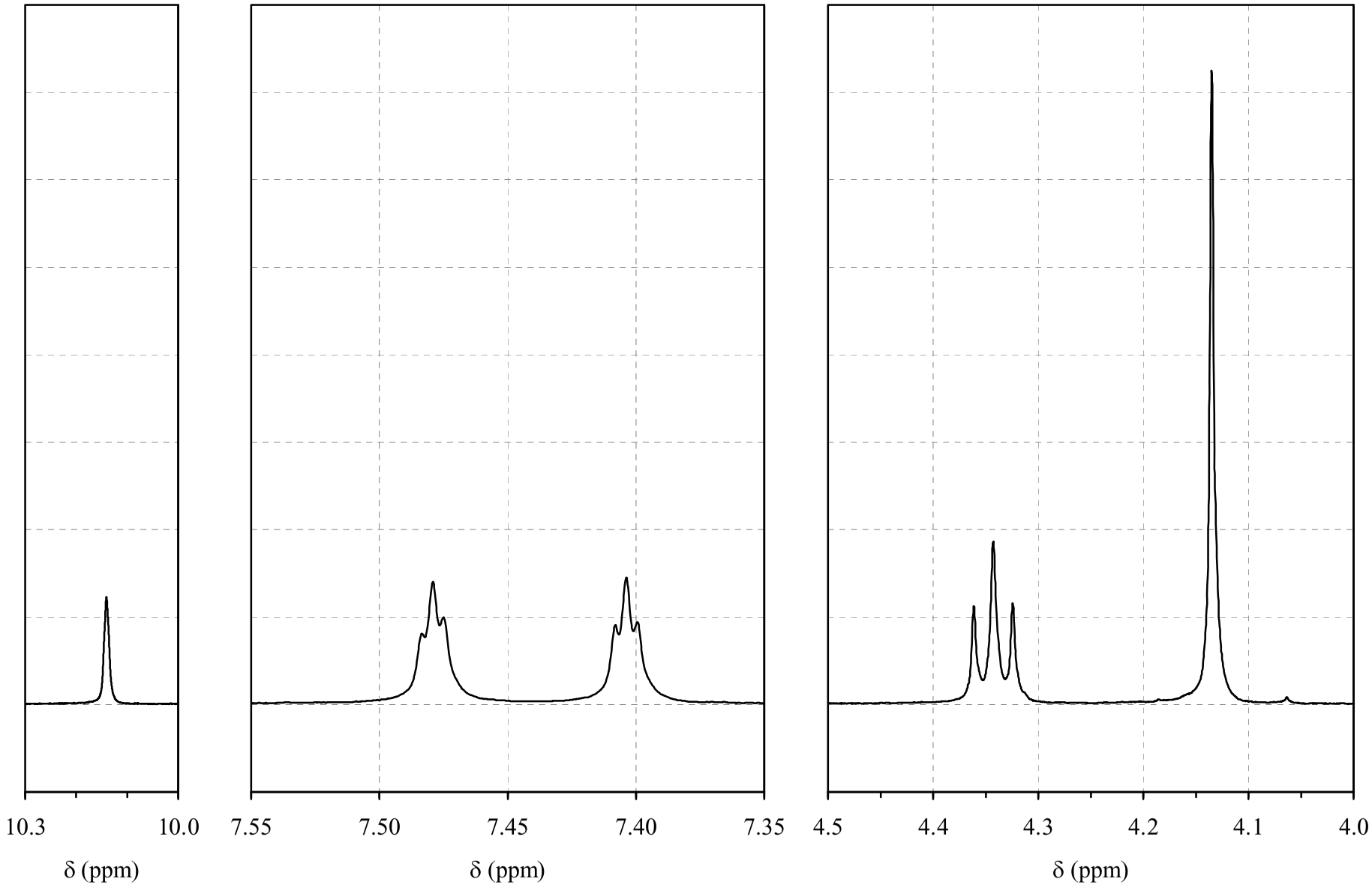

Figure S10. (c) ^{1}H NMR spectrum of 1-*n*-butyl-3-methylimidazolium iodide (BuMeImI).

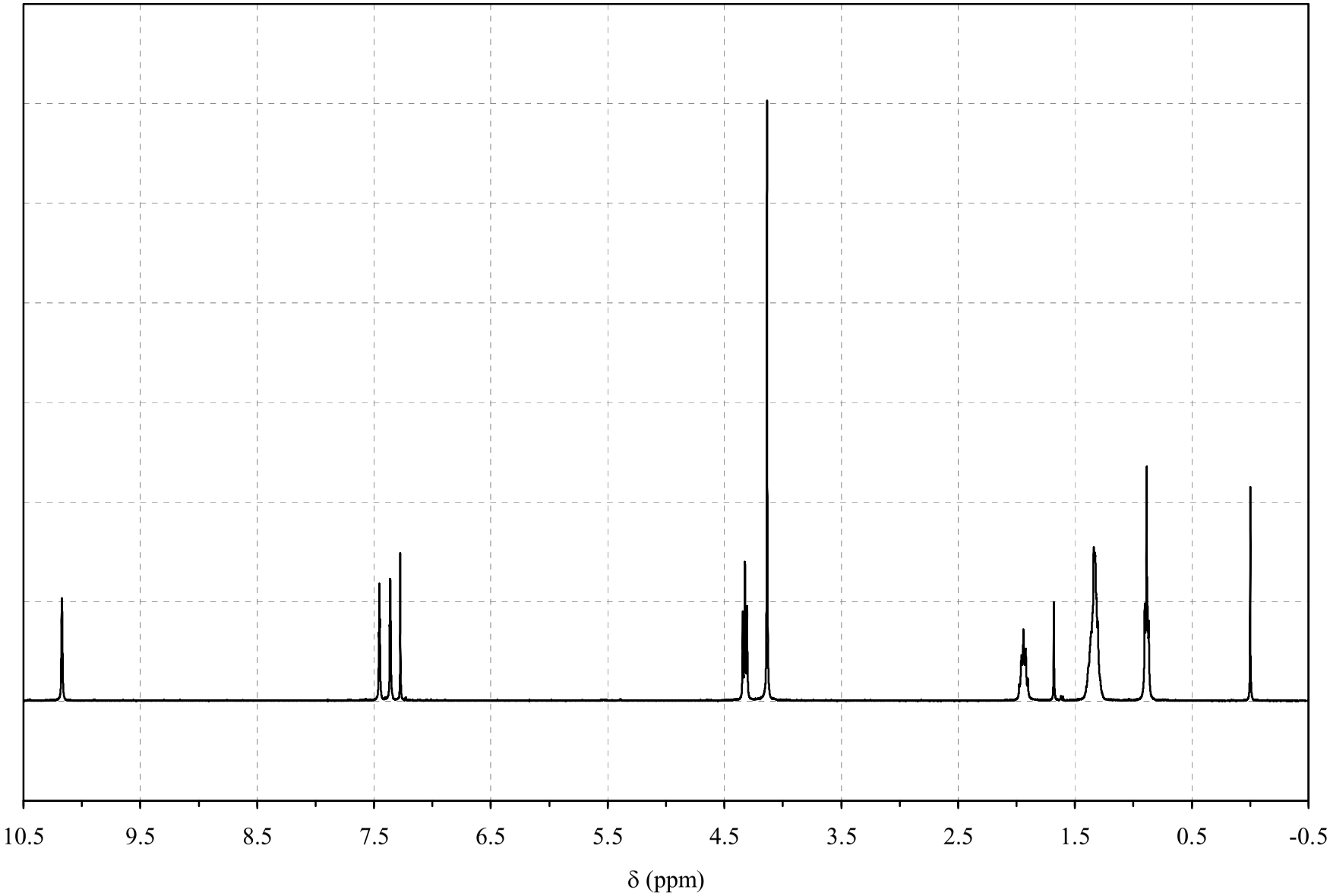

Figure S11. (a) ^{1}H NMR spectrum of 1-*n*-hexyl-3-methylimidazolium iodide (HexMeImI).

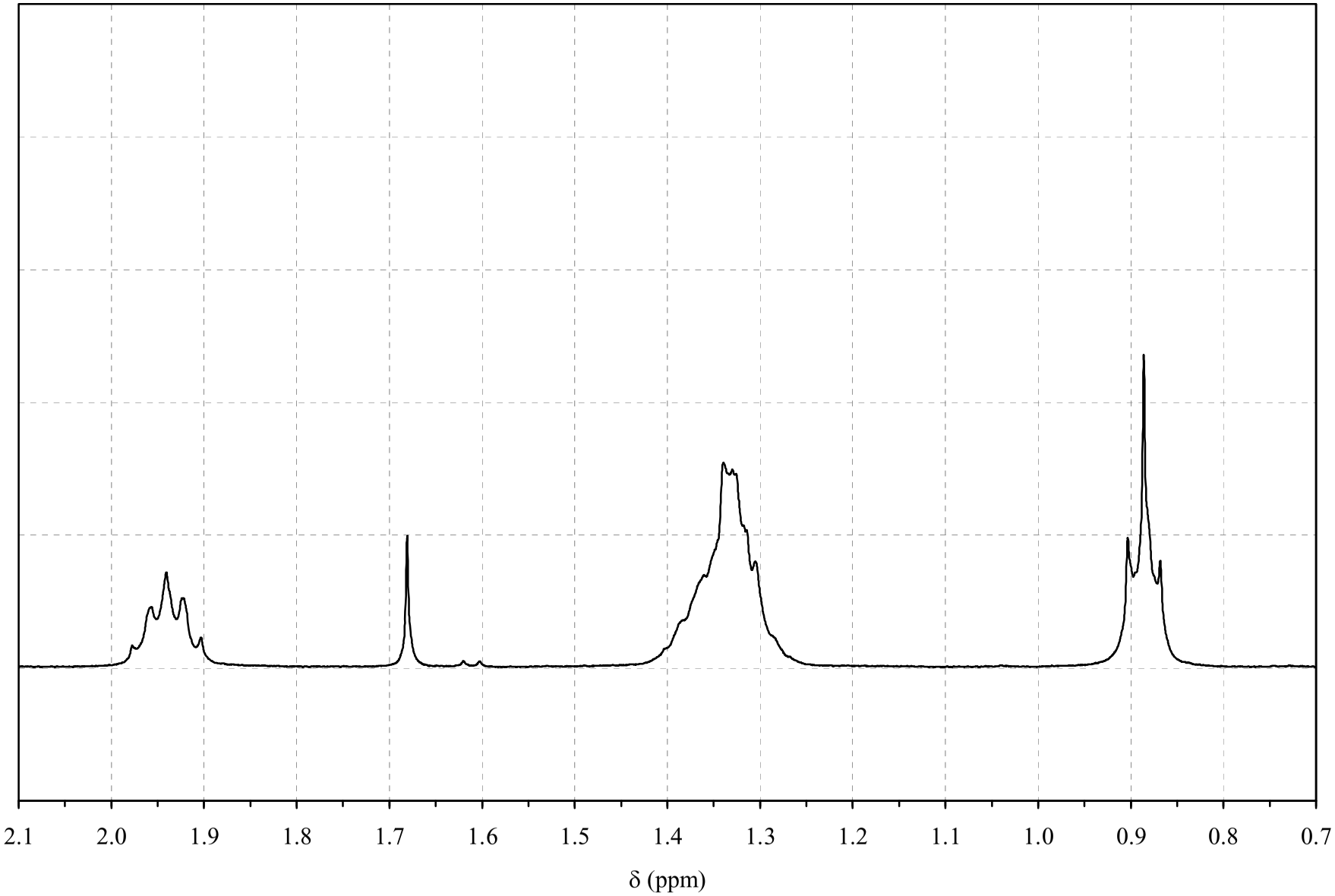

Figure S11. (b) ^{1}H NMR spectrum of 1-*n*-hexyl-3-methylimidazolium iodide (HexMeImI).

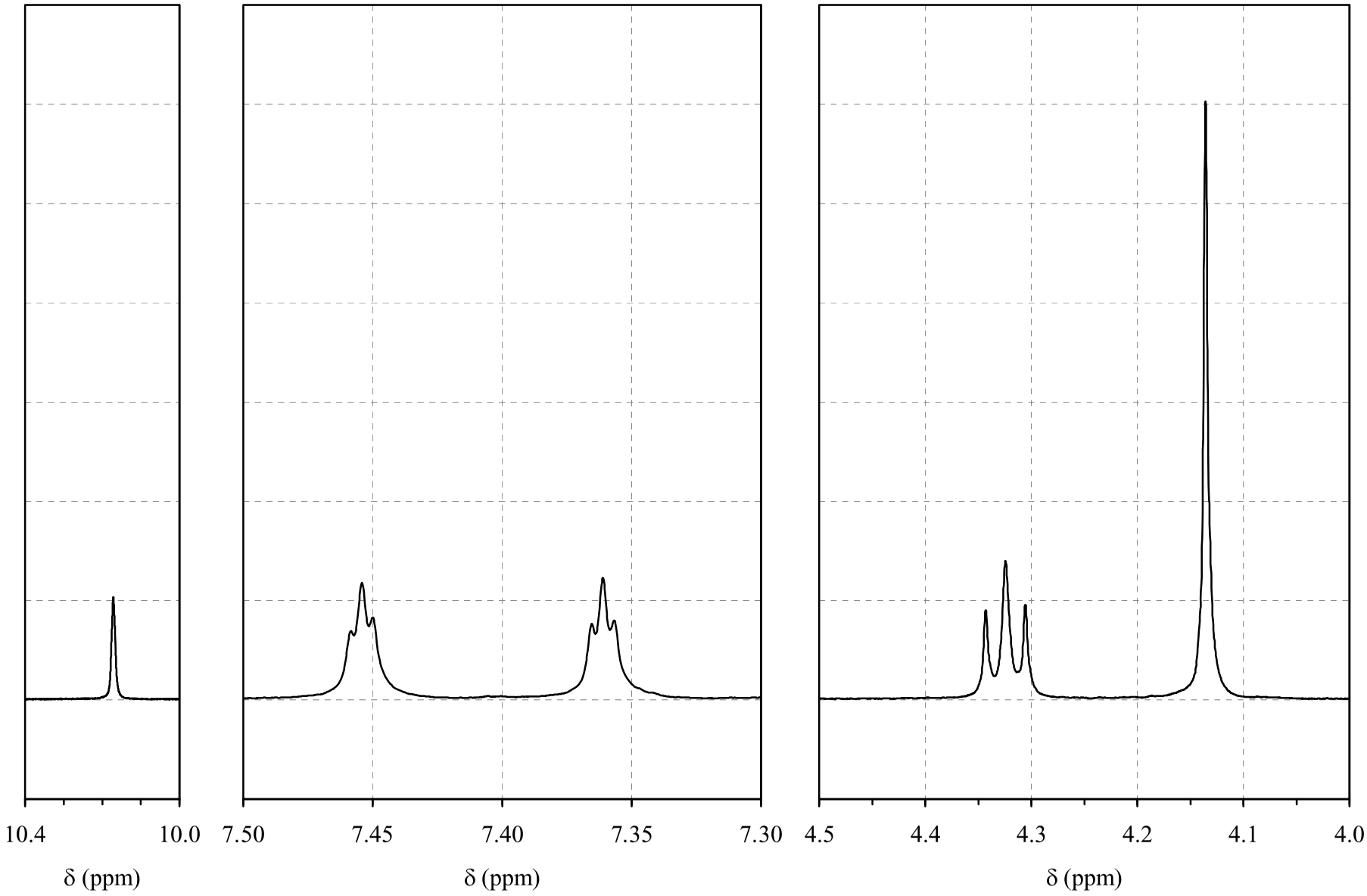

Figure S11. (c) ^{1}H NMR spectrum of 1-*n*-hexyl-3-methylimidazolium iodide (HexMeImI).

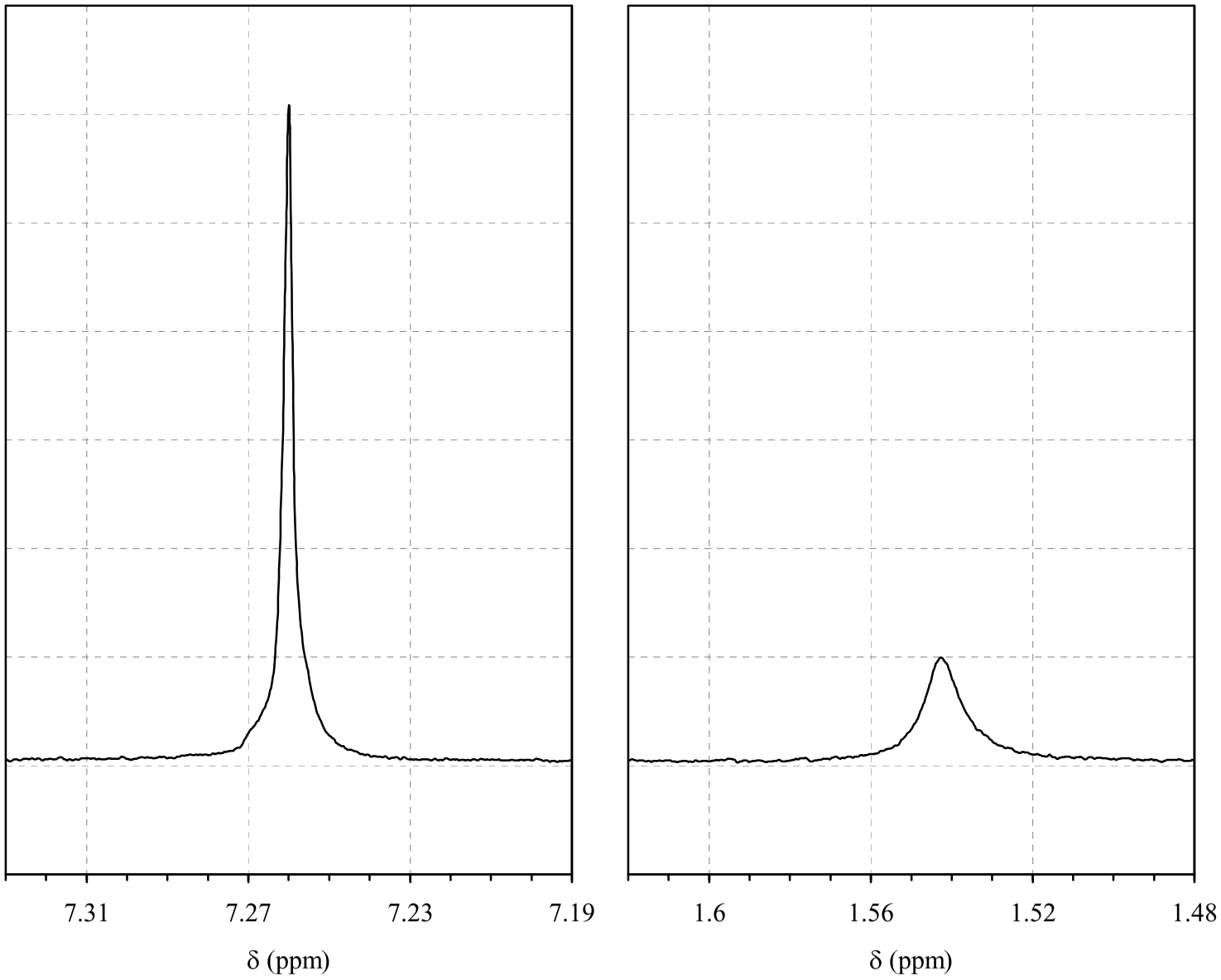

Figure S12. ^{1}H NMR spectrum of $CDCl_3$ solvent.

References

1. Reid, R. C.; Prausnitz, J. M.; Poling, B. E. The Properties of Gases and Liquids, 4th ed., McGraw-Hill: New York, 1987.

2. *Impedance Spectroscopy: Theory, Experiment, and Applications*, 2nd ed.; Barsoukov, E.; Macdonald, J. R. Eds.; Wiley-Interscience: New York, 2005.

3. Hanson, K. J.; Tobias, C. W. Electrochemistry of iodide in propylene carbonate, *J. Electrochem. Soc.* **1987**, *134*, 2204–2210.

4. Kupka, T. Complete basis set B3LYP NMR calculations of $CDCl_3$ solvent's water fine spectral details. *Magn. Reson. Chem.* **2008**, *46*, 851–858.

5. Sigma-Aldrich Webpage. Double Water Peaks in Deuterated NMR Solvents. http://www.sigmaaldrich.com (accessed August 2010).